DIFFRACTION OF LONG WAVELENGTH X-RAYS

by

Burton Henke

OFFICE OF NAVAL RESEARCH
Special Technical Report No. 24

and

ATOMIC ENERGY COMMISSION
Special Technical Report No. 3

FUNDAMENTAL RESEARCH IN SPECTROSCOPY OF X-RAYS AND GAMMA-RAYS

Contract No. N6onr-244, T.O. IV
(NR 017-602)

Contract No. AT(04-3)-8

Dr. Jesse W.M. DuMond
Contract Supervisor

CALIFORNIA INSTITUTE OF TECHNOLOGY PASADENA, CALIFORNIA

June 1953

This Special Technical Report discusses the theory and application of low-angle x-ray diffraction by long wavelengths.

Four methods of obtaining the diffraction pattern are described, namely (1) the double-crystal spectrometer, (2) the annular slit system, (3) the concave mica, point-focusing monochromator, and (4) the total-reflection, point-focusing system. The design and construction of the total-reflection equipment is described in detail. This method is applied to the measurement of the Dow latex particles.

The work described here is essentially the subject matter of a thesis for the Ph.D. degree in Physics of Mr. Burton Henke.

TABLE OF CONTENTS

TABLE OF CONTENTS (continued)

I. INTRODUCTION

The most direct way to evaluate the size and shape of a structure which is beyond the resolution of the light microscope is to use the electron microscope. The resolution of this instrument as set by lens aberrations is generally no better than 20 A. However, often particles as large as 500 A cannot be photographed because of their transparency to the electron beam. This is particularly true for organic samples. Shadow-casting techniques are used to circumvent this lack of scattering power, but sometimes this treatment changes the structure to the extent that an interpretation of size and shape is difficult. Another inherent limitation of the electron microscope lies in the great difficulty with which a calibration of the magnification is made. To date, there is no calibration technique which is of accuracy commensurate with the resolution of the electron microscope.

Another, less direct method for studying sub-light-microscopic structure is that of low-angle x-ray diffraction. In fact, this method may be applied to sub-electron-microscopic structure as well. In this approach, however, one does not study the structure of a single particle or individual, but rather one obtains information from the integrated effect of scattering from a great many particles or individuals. In one respect this is an advantage since the diffraction intensity distribution that is characteristic of the size and shape of a single unit is greatly intensified by the addition of patterns from all such units that make up the sample. The calibration of the diffraction camera lies simply in the measurement of its linear dimensions. This method could be used

to determine accurately the diameter of such uniform particles as the now well known Dow latex spheres, (580 G, lot 3584) which, in turn, may be used to calibrate the electron microscope.

The accuracy of such a measurement depends upon (1) the resolution afforded by the means adopted for measuring the diffraction pattern, and (2) the validity of the diffraction theory that is used. The applicability of the relatively straightforward Guinier theory[1] rests on the following assumptions; (1) The diffraction unit is so designed that the pattern which is formed is identical to that which would be formed by a parallel monochromatic beam of negligible cross-section. (2) Electron density fluctuations within a particle occur in regions that are small compared with a wavelength. (3) Effects due to absorption and refraction within the sample are negligible. (4) Effects due to multiple scattering and to multiple refractions are negligible.

The use of long wavelengths in low-angle diffraction methods is of considerable interest. The effects of multiple scattering, multiple refractions, and of electron density fluctuations become, or can be made, vanishingly small at these wavelengths. The larger angles of scattering for the long wavelengths permit the measurement of the very important central region of the diffraction pattern. And finally, the size of the particles and the thinness of the sample mounting appropriate to these wavelengths invite direct comparison studies with the electron microscope. Such studies might provide valuable information as to the nature of packing and other gross features of the material. A calibration of the electron microscope could be made from the

identical latex particle sample which had been accurately measured by the long wavelength diffraction method.

The purpose of the work which is described here has been the development of a long wavelength, low-angle diffraction method. This research was undertaken after two years of work with the electron microscope. A diffraction theory for the region of long wavelengths is discussed. Several modes of low-angle diffraction instrumentation are investigated. One of these, which utilizes total-reflection focusing, is developed in detail. This instrument is applied to the measurement of the Dow latex particles.

II. LONG WAVE DIFFRACTION THEORY

For ordinary x-rays at least, the shape of the low-angle diffraction pattern is completely independent of all the characteristics of the material except the particle size and shape. This is not true for the corresponding light scattering methods for which a size determination rests also on the knowledge of the index of refraction and the absorption coefficient. Perhaps this is the most important reason why low-angle x-ray diffraction is attractive for high precision measurements.

Somewhere between the ordinary x-ray and the ultraviolet regions this sensitivity to the characteristics of the material other than size and shape of particle structure becomes appreciable. The "unit difference" of the index of refraction for x-rays increases with the square of the wavelength, and the mass absorption coefficient with the cube of the wavelength. Therefore, it would seem appropriate that one should investigate first the effects of any second order terms to the ordinary x-ray diffraction theory in the development of a long-wavelength diffraction method.

In order to be specific, it is intended to treat only the diffraction of a plane wave by a homogeneous sphere of diameter which is large compared with the wavelength. This is the aspect of the theory which will be applied directly to the problem of measuring the Dow latex particles.

1. Diffraction by a Homogeneous Sphere - The Guinier Method

This relatively simple theory of diffraction of a plane

electromagnetic wave by a homogeneous sphere is based upon the assumption that absorption and refraction can be neglected. It is assumed that the primary wave within the sphere is just as it would be if the sphere were absent. The amplitude of the wave diffracted at any particular angle is then integrated over all the contributions from infinitesimal dipole scatterers distributed uniformly throughout the sphere. This was done in terms of the polarizability and finally in terms of the index of refraction of the material by Rayleigh[2] and Gans[3]. It was done by Guinier[1] in terms of Thomsonian-electron scatters. That their results are equivalent is demonstrated by replacing the index of refraction in the Rayleigh-Gans expression by its classical value for the x-ray region.

One may obtain the Guinier expression by simply integrating, over the limits of the sphere, the reflected amplitudes from differential planes of circular section and of thickness dz. The differential amplitude component would then be equal to the product of four factors as follows: (1) the Thomson amplitude scattered per electron, (2) the number of electrons per unit volume, (3) the volume of the circular reflecting plane, (4) cos kz - - where kz is the phase of the z-scattered component relative to the midsection plane, z = 0. See Fig. 1. Thus

$$A = 2\pi n A_e \int_0^R (R^2 - z^2) \cos kz \, dz \qquad (1)$$

This may be readily integrated (Jahnke-Emde VIII-8b)

$$A = (2\pi)^{3/2} n A_e R^3 \frac{J_{3/2}(u)}{u^{3/2}}, \quad u = kR \qquad (2)$$

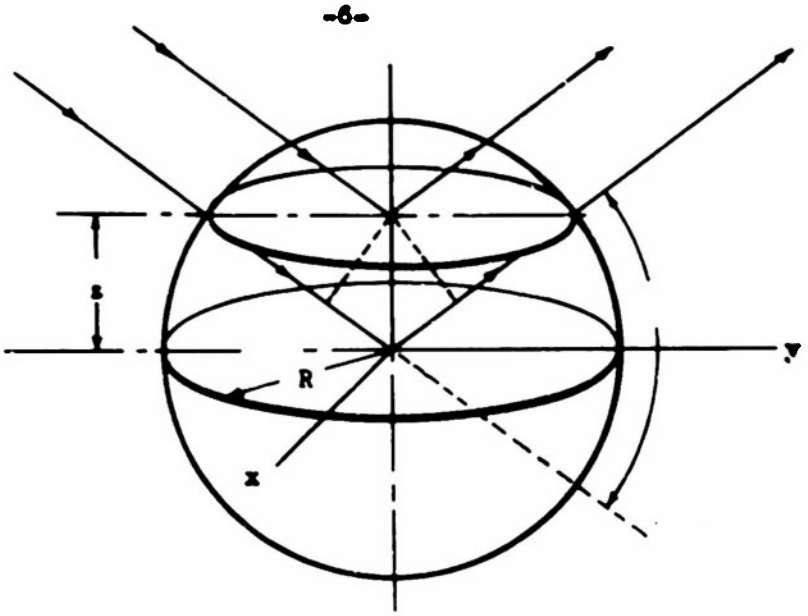

Fig. 6 Diffraction Geometry

Meaning of Symbols

ϵ - Angle of scattering

R - Radius of Particle

λ - Wavelength of incident radiation

$u = \frac{4\pi R}{\lambda} \sin(\epsilon/2)$

n - Number of electrons per unit volume

N - Total number of electrons per particle

δ - Unit decrement to the refractive index

u_m - Mass absorption coefficient

s_m - Mass scattering coefficient

Z - Atomic number

M - Atomic mass

Squaring the amplitude in order to derive the intensity, and recalling the Thomson expression for the intensity scattered per electron

$$I_e = |A_e|^2 = I_o \frac{e^4}{2r^2 m^2 c^4} (1 + \cos^2 \epsilon)$$

we obtain finally

$$I = I_o \frac{9\pi}{2} N^2 \left(\frac{e^4}{2r^2 m^2 c^4}\right)(1 + \cos^2 \epsilon) \frac{J^2_{3/2}(u)}{u^3} \qquad (3)$$

which is the Guinier distribution of intensity diffracted by a homogeneous sphere. A plot of $\left(J^2_{3/2}(u)/u^3\right) \times 10^8$ for values of u from 0 to 30 is shown in Fig. 2. The corresponding Rayleigh-Gans result may be written as

$$I = I_o \frac{8\pi^5 R^6}{r^2 \lambda^4} (m^2 - 1)^2 \left(\frac{1 + \cos^2 \epsilon}{2}\right) \frac{J^2_{3/2}(u)}{u^3} \qquad (4)$$

If we let $m - 1 = \delta = \frac{n e^2 \lambda^2}{2\pi m c^2}$ (the Drude-Lorentz classical result), we obtain an expression which is identical to (3).

It is interesting to note that this substitution for δ is valid only when the incident radiation is of wavelength that is not close to a critical absorption wavelength of the material particle. Unless this condition obtains it may not be possible to consider the scattering electron as entirely "free".

2. The Validity of the Guinier Diffraction Theory for Long Wavelengths

Since refraction and absorption effects increase rapidly with

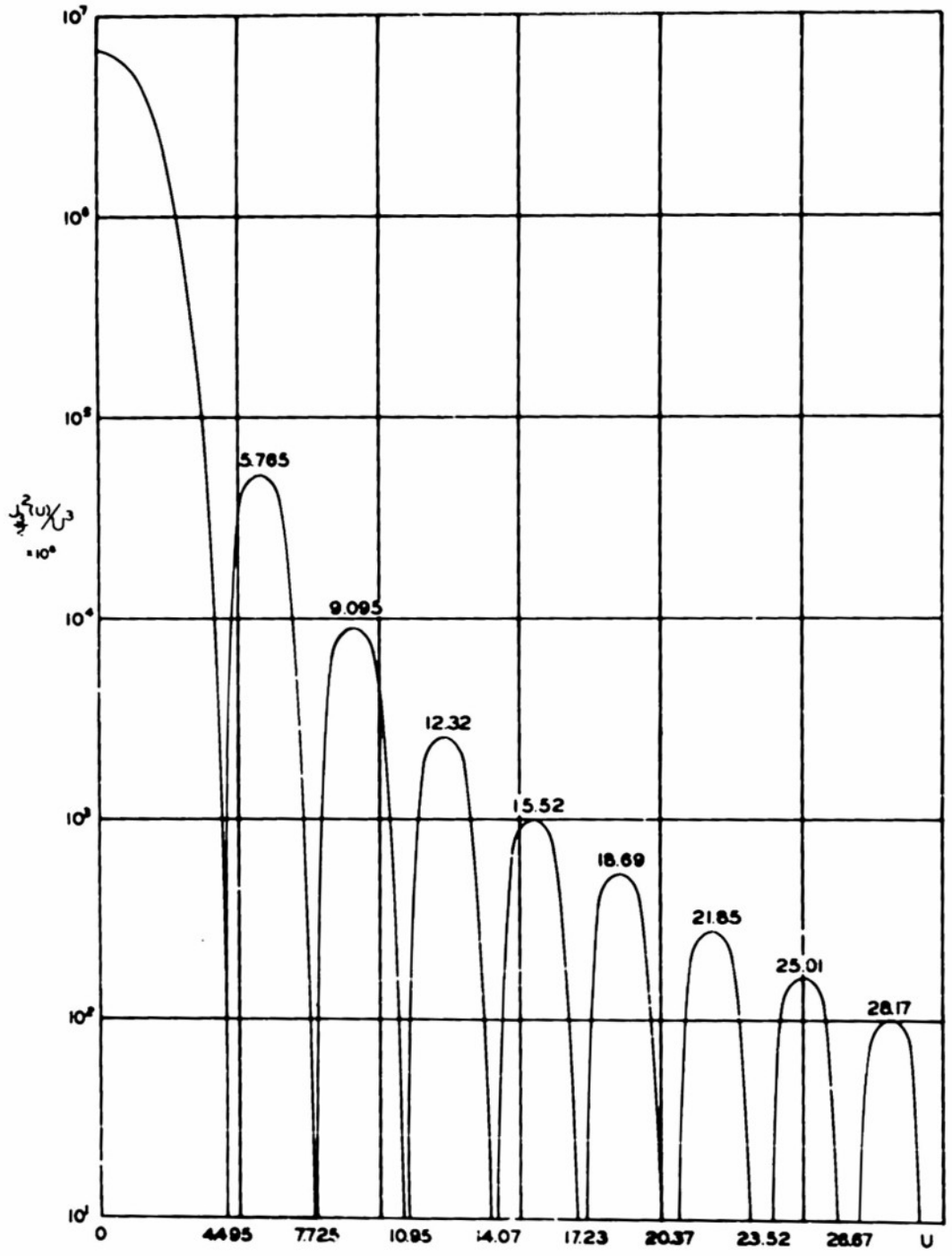

Fig. 2 Maxima and minima of diffracted intensity distributed for a spherical particle

wavelength, the question arises as to whether or not these effects may be neglected for the long wavelength x-ray region. To answer this question we must return to an exact solution of the problem derived from the application of Maxwell's equations. The exact solution for the diffraction of a plane electromagnetic wave by a homogeneous sphere was first solved by Mie[4]. In their texts, Smythe[5] and Stratton[6] outline the solution. This is given in infinite series form in terms of Legendre polynomials with coefficients involving spherical Bessel functions. Because of the importance of these solutions for light scattering applications[7], they have been extensively tabulated[8]. Debye[9] and van de Hulst[10] have developed different forms of these solution which are more amenable to analysis. It is a straightforward matter to obtain Guinier's expression for the limiting case for which the index of refraction approaches unity from van de Hulst's work. However it would seem most satisfactory to start from a reduction of the Mie theory to equations of closed form which has recently been accomplished by Hart and Montroll[11] for scattering by "soft spheres". Their solutions become exact as the index of refraction approaches unity, and do yield the Guinier expression for the ordinary x-ray region as would be expected.

Now in order to obtain from their result terms which may be regarded as second order corrections to the Guinier expression we replace the index of refraction, m, by $1 - \gamma$ where γ is given by $\gamma = \delta + i\beta$, the sum of the real and the imaginary increments. The latter introduces the effect of absorption. Since $|\gamma| \ll 1$ we may immediately rewrite their result as

$$\frac{I_s}{I_o} = \frac{\pi R^2 x^4}{r^2} |\gamma|^2 (1+\cos^2\epsilon) \left\{ \frac{J_{3/2}(wx)}{(wx)^{3/2}} - \frac{\gamma e^{ix}}{2} \frac{J_{3/2}(vx)}{(vx)^{3/2}} \right\}^2 \quad (5)$$

in which $x = 2\pi R/\lambda$ and for the x-ray region of interest where $\beta \ll \delta \ll 1$ and where $\sin\epsilon$ may be replaced by ϵ in correction terms, we may express $w = 2 \sin \epsilon/2(1 - \frac{1}{2}(\delta/\epsilon)^2)$ and $v = 2 \cos \epsilon/2$. Since then $v >> w$ and $|\gamma| << 1$, we may neglect the second term in the parenthesis. Thus, the above expression may be written as

$$\frac{I_s}{I_o} = \frac{\pi R^2 x^4}{r^2} \delta^2 \left(1+\left(\frac{\beta}{\delta}\right)^2\right)\left(1+\cos^2\epsilon\right) \frac{J^2_{3/2}\left[u\left(1+\frac{1}{2}\left(\frac{\delta}{\epsilon}\right)^2\right)\right]}{u^3\left(1+\frac{1}{2}\left(\frac{\delta}{\epsilon}\right)^2\right)^3}$$

which is the Guinier expression plus the second order terms. In order to compute these corrections to the Guinier diffraction pattern we use the Drude-Lorentz expression for

$$\delta = \frac{n e^2}{2\pi m c^2} \lambda^2 = 2.70 \times 10^{-6} \frac{\rho Z}{M} \lambda^2 \quad (7)$$

and the classical expression for β (Compton and Allison, p 278)

$$\beta = \frac{10^{-8}}{4\pi} \mu_m \rho \lambda \quad (8)$$

in which λ is to be expressed in A.U. We then obtain

$$\frac{1}{2}\left(\frac{\delta}{\epsilon}\right)^2 = .91 \times 10^{-12} \left(\frac{2Z}{M}\right)^2 \left(\frac{\rho^2 \lambda^4}{\epsilon^2}\right) \quad (9)$$

and

$$\left(\frac{\beta}{\delta}\right)^2 = 3.5 \times 10^{-7} \left(\frac{M}{2Z}\right)^2 \left(\frac{\mu_m}{\lambda}\right)^2 \qquad (10)$$

The refraction correction (9) increases rapidly for very small angles of scattering, and for a given relative angular position, it increases with λ^2. The absorption effect increases with Z^6 and λ^4 since μ_m is approximately proportional to $(Z\lambda)^3$.

Below are tabulated the numerical values of these corrections for two systems of particles which have been of interest, the latex particles and gold sols. These are computed for a typical "ordinary" wavelength, Cu K_α (1.54 A) and for a long wavelength, O-K_α (23.6 A). The refraction correction is referred to the inflection point of the central maximum and to the position of the first secondary maximum.

It should be noted that the refraction correction is equal to the relative error in a measurement of R, if this correction is not made.

Sample	λ	Refraction Correction $\left(\frac{1}{2}\left(\frac{\delta}{\epsilon}\right)^2\right)$		Absorption Effect
		Inflection Point	1st Secondary Maximum	$\left(\frac{\beta}{\delta}\right)^2$
Dow latex particles	1.54	$1.5\ 10^{-4}$	$8.6\ 10^{-6}$	$3.5\ 10^{-6}$
R = 1350 A	23.6	$3.7\ 10^{-2}$	$2.1\ 10^{-3}$	$6.\ 10^{-2}$
Gold Sol	1.54	$5.6\ 10^{-4}$	$3.2\ 10^{-5}$	$7.8\ 10^{-3}$
R = 250 A	23.6	.14	$.8\ 10^{-2}$	.2

The following conclusions may now be drawn from the above results:

(1) The Guinier theory does accurately predict the shape of the diffraction pattern for ordinary x-rays such as Cu-K_α (1.54 A), to within a maximum error of about one tenth of one percent. Since the maximum absorption effect is merely to increase the intensity of the pattern by about one percent, this effect is wholly negligible for usual applications with ordinary x-rays. However, the total power scattered may drop appreciably for any wavelength that is very near to a critical absorption edge for the scattering material.

(2) For long wavelength diffraction a refraction correction may well be necessary as indicated above by the nearly fifteen percent shift in the diffraction pattern near the inflection point of the pattern for 250 A gold sol, using 23.6 A radiation. Since, however, this effect is proportional to ρ^2, it would be entirely negligible even at this wavelength for organic samples. At long wavelengths the absorption effect does appreciably increase the total power scattered by dense materials, e.g., twenty percent increase for gold using 23.6 A.*

(3) Refraction effects will be negligible as long as $\delta R \ll \lambda$. If a correction is necessary, it is relatively easy to apply, and does not require a very precise knowledge of the refractive index.

In the analysis of multiple scattering and multiple refraction that follows, the usual Guinier expression will be used. Its form in (3) may be rewritten as:

---

* It is interesting that the first effect of absorption within the sample is to produce a diffraction pattern identical to that produced by scattering. This has the analogy, of course, in the operation of the Babinet principle for aperture vs screen diffraction.

$$I = C\, I_o \frac{J_{3/2}^2(u)}{u^3} \tag{11}$$

in which

$$C = \frac{\pi R^2 x^4}{r^2} \delta^2 \left(1 + \left(\frac{\beta}{\delta}\right)^2\right)(1 + \cos^2 \epsilon)$$

and for $M \approx 2Z$, $\cos\epsilon \approx 1$,

$$C \approx (1.78 \times 10^{-24}) \frac{\rho^2 R^6}{r^2} = K \frac{\rho^2 R^6}{r^2} \tag{12}$$

3. The Mass Scattering Coefficient for Low-Angle Diffraction

Before we can determine the effects of multiple scattering, we must first calculate the total power scattered in the diffraction pattern and the scattering cross section.

The total power scattered is obtained by integrating the intensity over a spherical area which includes all of the pattern. Thus

$$P = \int I(\epsilon)(2\pi r^2 \sin\epsilon\, d\epsilon) = K\, I_o \rho^2 R^6 (2\pi) \int \frac{J_{3/2}^2(u)}{u^3} \sin\epsilon\, d\epsilon$$

But we may write

$$\sin\epsilon\, d\epsilon = 4 \sin\left(\frac{\epsilon}{2}\right) \cos\left(\frac{\epsilon}{2}\right) d\left(\frac{\epsilon}{2}\right)$$

and since $u = \frac{4\pi R}{\lambda} \sin\frac{\epsilon}{2}$

$$4 \sin\frac{\epsilon}{2} \cos\frac{\epsilon}{2}\, d\left(\frac{\epsilon}{2}\right) = \frac{1}{4\pi^2}\left(\frac{\lambda^2}{R^2}\right) u\, du$$

we have finally

$$P = \frac{K}{2\pi} \; I_o \rho^2 \; R^4 \; \lambda^2 \int_0^\infty \frac{J_{3/2}^2(u)}{u^3} \, d\,u$$

The infinite limit is justified by the very rapid way with which the integrand approaches zero as u becomes large. This expression is readily integrated (Watson, Bessel Functions 13:41) and we obtain

$$P = \frac{K \; I_o}{4\pi^2} \; \rho^2 \; R^4 \; \lambda^2 \tag{13}$$

And the particle cross section for low-angle diffraction is

$$S_p = \left(\frac{P}{I_o}\right) = \frac{K}{4\pi^2} \; \rho^2 \; R^4 \; \lambda^2 \tag{14}$$

The cross section per gram is the product of the number of particles per gram and the cross section per particle. Thus

$$S_m = \left(\frac{1}{\frac{4}{3} \; \pi \; R^3 \rho}\right) S_p = \frac{3K}{16 \; \pi^3} \; \rho \; R \; \lambda^2 \tag{15}$$

By using (12) we obtain

$$S_m \approx 0.011 \; \rho R \; \lambda^2 \tag{16}$$

in which R and λ are expressed in A.U.

4. The Mass Absorption Coefficients for Long Wavelengths

We shall also need values for the long wavelength absorption

coefficients in order to determine the effect of multiple scattering and to obtain a criterion for sample thickness.

Very little work has been done on the measurement of mass absorption coefficients in the long wavelength region. Compton and Allison[12] have published Allen's compilation of the work of Jönnson[13], of Dreshem and Shein[14], and of Woernle[15]. Later work on absorption of long wavelengths in aluminum has been published by Bandopadhyaya and Maitra[16], who have found that $\mu_m = C\ \lambda^{2.95}$ for Al and for wavelengths from 7 to 24 A.U.

Victoreen[17] has used Allen's compilation of absorption coefficients to determine the constants in a semi-empirical equation which he then uses to complete a table for μ_m as a function of atomic number and wavelength. These values of μ_m, however, are only for wavelengths below the critical K-absorption wavelengths and consequently include only the long wavelength data for the light elements.

In order to learn whether or not there exists a simple power law relationship for the mass absorption coefficient as a function of atomic number, $\log \mu_m$ was plotted against $\log Z$ for 8.32, 11.9, 13.3, 23.6, and 44.5 A.U., using all available values for μ_m. The values for each wavelength were satisfactorily fit by a straight line on both sides of the critical K-absorption point. All such lines for all five wavelengths have nearly the same slope, which is approximately equal to 2.65. We conclude, therefore, that an expression which will give the absorption coefficient for wavelengths in the 10 to 25 A.U. range within a first order of approximation is

$$\mu_m = C\ \lambda^{2.95}\ Z^{2.65} \qquad (17)$$

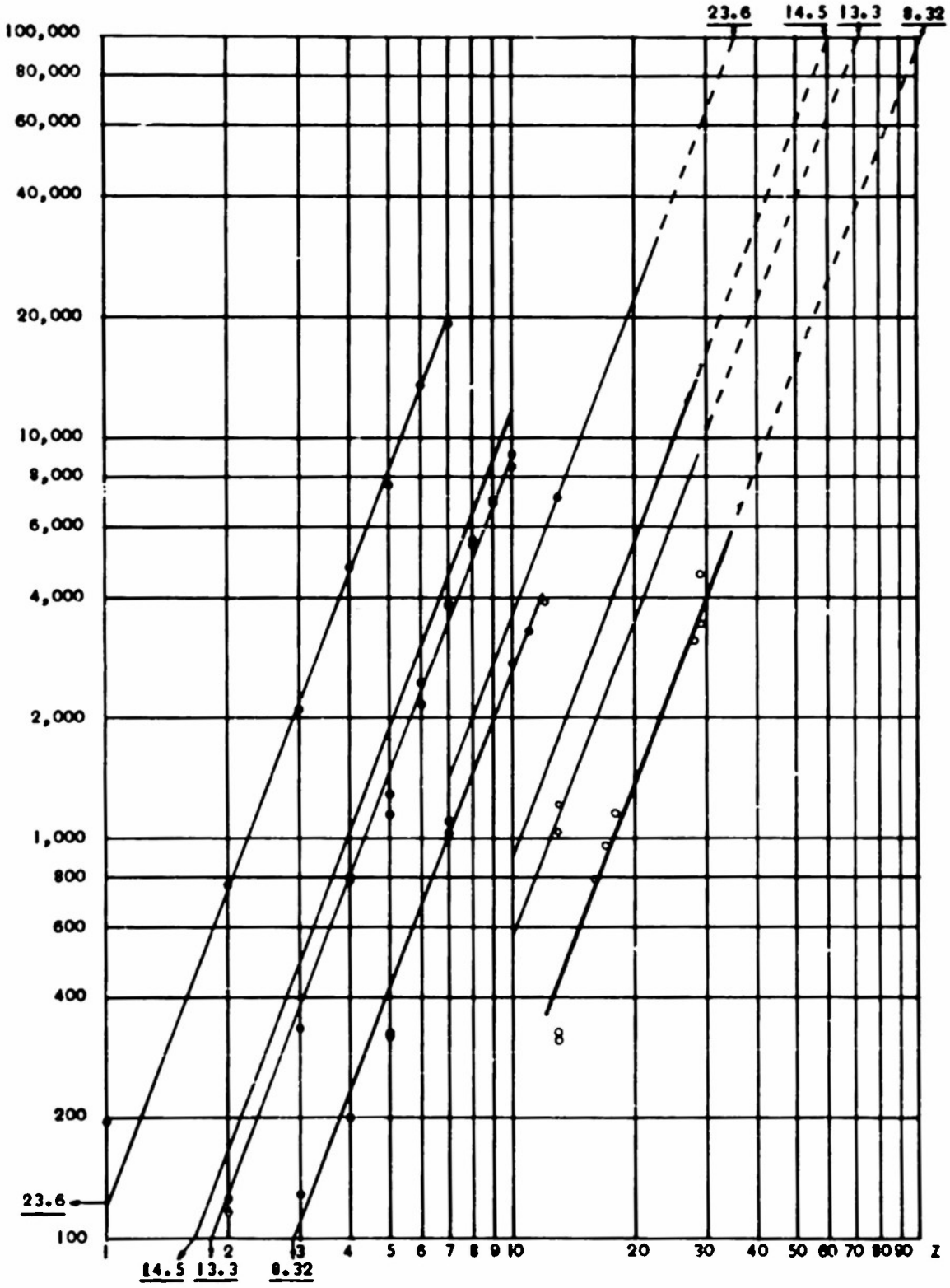

Fig. 3 MASS ABSORPTION COEFFICIENT

In Fig. 3 the mass absorption coefficients are plotted against the atomic number of the absorber for Al-K (8.32 A), Cu-L (13.3 A), Ni-L (14.5 A), and O-K (23.6 A) using (17) to obtain the curves for Ni-L (14.5 A) radiation.

5. Multiple Scattering in Low-Angle Diffraction

We shall calculate first the shape of the second-scattered intensity distribution. This component would, of course, be the strongest for low-order multiple scattering; that is, it would be much larger than the third scattered component, etc. It will be necessary to compute the distribution of the scattered intensity from a spherical particle which receives an incident intensity that is made up of components from first-scatterers which are behind this particle. These components are proportional to the value of the first-scattered intensity distribution function for the angle ϕ, which is the angle between the incident beam direction and this first-scattered component at the second-scatterer. See Fig. 4-a. The first-scattered component also depends upon the distance of the first scatterer to the second-scatterer, but for a uniform sample this dependence will not involve ϕ. It will be assumed that these particles are far enough away that the first-scattered waves are plane. Then the second-scattered intensity will be proportional to the integral

$$I_2 \propto \int_0^\infty I(\epsilon - \phi)\, I(\phi)\, d\phi$$

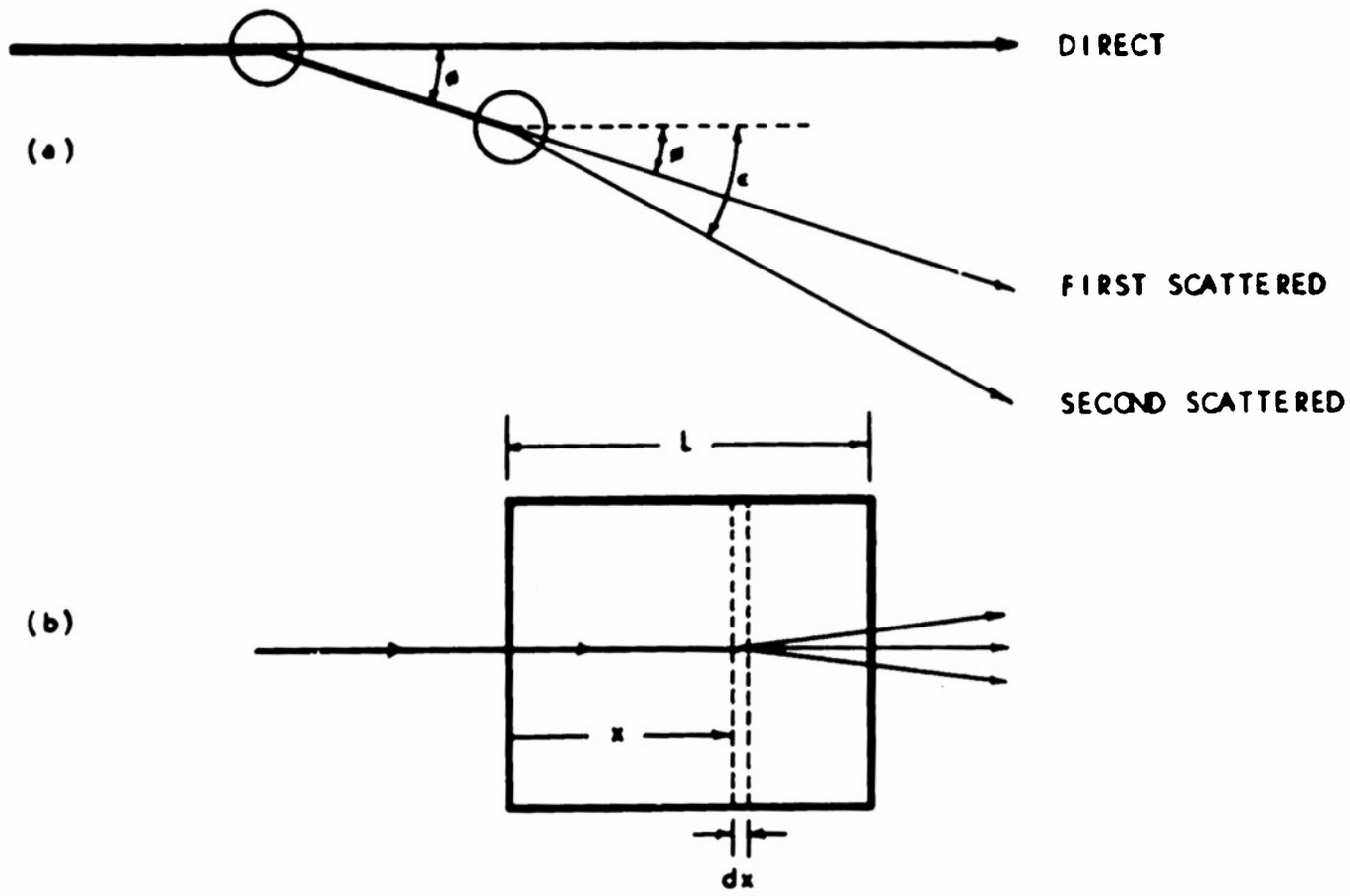

Fig. 4 SECOND SCATTERING GEOMETRY

in which I is the first-scattered intensity distribution derived above. Since only the strong central portion of the scattering will be important in second-scattering, it would be sufficient here to use the exponential approximation to the exact distribution, (11), which has been derived by Guinier[1]. Thus (11) may be approximated as

$$I_1 = \left(\frac{2}{9\pi}\right) K I_o \frac{\rho^2 R^6}{r^2} e^{-\frac{x^2 \epsilon^2}{5}} \tag{17}$$

and the desired integral becomes

$$I_2 \propto \int_0^\infty e^{-\frac{x^2}{5}\phi^2} e^{-\frac{x^2}{5}(\epsilon - \phi)^2} d\phi$$

Integrating, we obtain

$$I_2 \propto e^{-\frac{x^2 \epsilon^2}{10}} \int_0^\infty e^{-\frac{2x^2}{5}\left(\phi - \frac{\epsilon}{2}\right)^2} d\phi \propto e^{-\frac{x^2 \epsilon^2}{10}}$$

Then the second-scattered intensity distribution may be written as

$$I_2 = C e^{-\frac{x^2 \epsilon^2}{10}}$$

in which C does not depend upon ϵ and may be determined in terms of the scattering coefficient as will be shown below. We note that the second-scattering produces another Gaussian distribution which is broader than that of first-scattering by a $\sqrt{2}$ factor.

Let us now consider the effect of a thick sample with respect to both the first and second scattered components. The total mass

absorption coefficient will be $\mu_{tm} = \mu_m + s_m$, and we shall let $\mu_t = \mu + s$ denote the corresponding linear absorption coefficient for the sample material. We consider first the amount of first-scattered intensity that leaves an element of unit area and thickness dx within the sample and reaches the region outside the sample. See Fig. 4b. This is

$$d\,I_{1t} = I_o\, e^{-\mu_t x}\,(s\,dx)\, e^{-\mu_t (L-x)}$$

Integrating, we obtain the total intensity of the "pure" first-scattered component

$$I_{1t} = (sL)e^{-\mu_t L} I_o = (s_m m)\, e^{-\mu_{tm} L} I_o \qquad (18)$$

in which m is the mass per unit area of sample.

Similarly, the total intensity of second-scattered radiation that emerges from the sample is derived from

$$d\,I_{2t} = (sx)\, e^{-\mu_t x}\,(s\,dx)\, e^{-\mu_t (L-x)}$$

and

$$I_{2t} = \frac{1}{2}(sL)^2\, e^{-\mu_t L} I_o = \frac{1}{2}(s_m m)^2\, e^{-\mu_{tm} m} I_o \qquad (19)$$

From (18) and (19) we may obtain the ratio of the total power that is second-scattered to that which is first-scattered.

$$\frac{P_{s2}}{P_{s1}} = \frac{1}{2}(s_m m) \qquad (20)$$

Integrating the first scattered intensity distribution function over

the spherical area included in the pattern and equating this to the total power that is first-scattered from (18), we obtain

$$2\pi r^2 \int_0^\infty I_{01}\, e^{-\frac{x^2 \epsilon^2}{5}}\, \epsilon\, d\epsilon = s_m m\, e^{-\mu_{tm} m}\, I_o = \frac{5\pi r^2}{x^2}\, I_{01}$$

Therefore the first-scattered intensity distribution for a thick sample is

$$I_1 = \frac{x^2}{5\pi r^2}\,(s_m m)\, e^{-\mu_{tm} m}\, I_o\, e^{-\frac{x^2 \epsilon^2}{5}} \qquad (21)$$

The scattering coefficient s_m is given from (15).

In a similar way we may obtain the second-scattered intensity distribution for a thick sample,

$$I_2 = \frac{x^2}{5\pi r^2}\, \frac{(s_m m)^2}{4}\, e^{-\mu_{tm} m}\, I_o\, e^{-\frac{x^2 \epsilon^2}{10}} \qquad (22)$$

And the ratio of the power that is second-scattered to that which is first-scattered at a particular angle becomes

$$\frac{I_2}{I_1} = \left(\frac{s_m m}{4}\right) e^{\frac{x^2 \epsilon^2}{10}} \qquad (23)$$

Setting $dI_1/dm = 0$ in (18) we obtain the value for the mass per unit area of sample that will yield maximum first-scattered intensity. This is

$$m = \frac{1}{\mu_{t_m}} = \frac{1}{\mu_m + s_m} \qquad (24)$$

Doing the same for I_2 from (19) we note that the value of m that results in maximum second-scattered intensity is just twice this thickness.

Many workers have used the $\frac{1}{\mu_t}$ thickness for their low-angle diffraction sample mounting. In fact some have used calculated $1/\mu$ thicknesses which neglects the contribution of small-angle scattering to the total absorption coefficient. That these practices result in an appreciable amount of second-scattering along with the first-scattered intensity distribution is shown by computing the ratio of the second-scattered power to that which is first-scattered for two samples, the Dow latex particles and 250 A carbon black.

	Latex Particles R = 1350 A		Carbon Black R = 250 A	
Wavelength	1.54	23.6	1.54	23.6
Scattering Coefficient, s_m	47.4	$1.1\ 10^4$	11.8	$2.8\ 10^3$
Mass Absorption Coefficient, μ_m	4.52	10^4	4.52	10^4
P_2/P_1 for $1/\mu$ thickness	5.0	0.5	1.3	0.14
P_2/P_1 for $1/\mu + s)$ thickness	.48	.25	.36	.11

The nature of multiple scattering is such as to "smear" out the first-scattered distribution thus obliterating the secondary maxima in the second-scattered distribution. Often the secondary maxima from first-scattering can be detected above a relatively large amount of more or less continuous second-scattered background. The shift in the

positions of the peaks due to the presence of the background is easily corrected for. Therefore it is conceivable that if one is concerned only with the position of secondary maxima the amount of second-scattering that is associated with $1/\mu_t$ sample thickness, as indicated above, could be tolerated.

Usually, however, one does not have the uniformity of particle size that is necessary to obtain these secondary maxima even in first-scattering. And the problem then is to determine the size distribution as well as the size from information that is obtained from the central region only. In this case, $1/\mu_t$ thickness would yield a very erroneous intensity distribution. In fact the sample thickness should be determined by the rule that

$$P_2/P_1 = \frac{1}{2} s_m \, m \ll 1 \qquad (25)$$

which usually gives a value of m considerably less than $1/\mu_{tm}$

Unfortunately, the power scattered is also proportional to (s_m) and is therefore reduced considerably along with the reduction of second-scattering. This fact explains and emphasizes the need for a high intensity, and a high intensity-to-background ratio for the diffraction unit.

6. The Multiple Refraction Effect

One of the first descriptions and applications of small angle scattering by microscopic particles was by von Nardroff[18] in 1926. He considered the x-ray beam to be refracted by each spherical particle as though it were a small lens. Thus as regards its angular distribution,

the pattern from an individual particle would depend only upon the index of refraction and not upon the size of the particle. However, for the case of multiple refraction, the pattern is broadened much as was described above for multiple scattering, and this broadening was considered a function of the number of refractions. For the refraction indices extremely close to unity as considered by von Nardroff a huge number of repetitions of the process, as the beam traversed successive particles, were required to produce a measurable enlargement of the pattern. Assuming that the enlargement of the primary beam was due to this effect alone (thus completely ignoring low angle diffraction) von Nardroff deduced in this way the number of particles through which the beam passed. Knowing the thickness and density of the material, it was then possible for him to compute the inferred radius of the particles.

However, as we have already shown, for particles which are below the light-microscopic range, for which the relation $\delta R \ll \lambda$ is almost invariably true, the diffraction of the beam is nearly the complete cause for the scattering, and refraction is negligible. And if the refraction broadening were not negligible it could be included in the scattering coefficient by integrating the more exact scattering function -- the above analysis for multiple scattering would still apply.

7. The Packing Effect - Inter-Particle Interference

A final mechanism that might distort the diffraction pattern from that expected for a single sphere would be that of inter-particle interference. A regular spatial arrangement of any sort will change

the intensity distribution from that for a single particle or for randomly spaced particles. And this effect is most marked in the central portion of the pattern which is usually the region of greatest interest. The effect of this inter-particle interference in the measurement of the latex particles is discussed by Danielson, Shenfil, and DuMond[19].

The effect of the inter-particle interference which "measures" the packing of the particles may be separated from the effect of the diffraction component which "measures" the size of the particles provided the type of packing is known. Otherwise one must guess as to what is a reasonable packing model and check its validity by indirect means.

8. The Advantages of Long Wavelength Diffraction

Because of the high absorption and scattering coefficients for the long wavelengths in the region of 15 to 25 A, low-angle diffraction samples as the Dow latex should consist of mono-particle layers mounted on thin films very much as for the electron microscope. This type of mounting has several advantages: (1) Multiple scattering is eliminated. (2) One may gain more control of the dispersing of the particles, using the same techniques[20] that have been used in electron microscopy. For particles smaller than the Dow latex particles which one might wish to be in double-layers, for example, the sample could be built up of two mono-layers one on each side of the supporting film, thus insuring randomness. (3) The same sample or one that is mounted in an identical manner to that which is used for the low-angle

diffraction study may be then studied with the electron microscope for useful "gross" information. The nature of packing can thus be determined, if the particles are not observed to be randomly distributed, and in turn, this effect can be taken into account in the size determination by the low-angle diffraction method. A direct check on size distribution for the sample that is used in the diffraction camera may also be gained in this way. (4) Such thin samples require relatively small amounts of sample material. This is an important consideration with certain types of virus investigations, for example.

The larger angles of scattering associated with the long wavelengths bring the important central portion of the diffraction pattern out of the vicinity of the direct beam. When the diffraction intensity is so weak as to be barely measurable above background, these larger angles permit the effective use of stops near the sample to reduce this background.

Finally, as will be described in Part IV, the instrumentation for long wavelength diffraction can be made relatively simple, yet with satisfactory intensity, resolution, and monochromatization.

III. DIFFRACTION UNITS

The principal requirement for a diffraction unit is that it form a diffraction pattern which is identical to that which would be formed by a monochromatic, parallel beam of negligibly small cross section. This need for high resolution and good monochromatization is very strong because of the requirement for precise data imposed by the necessity of "unfolding" or otherwise correcting the observed diffraction pattern with respect to effects such as inter-particle interference, size distributions, or with respect to the usually subtle changes in the diffraction due to a non-spherical shape of the particles. Since R is calculated from the diffraction parameter $u = \frac{2\pi R}{\lambda}\epsilon$, we note that the relative deviation in R as a function of the monochromatization of the primary radiation and angular resolution becomes

$$\frac{\Delta R}{R} = \sqrt{\left(\frac{\Delta\lambda}{\lambda}\right)^2 + \left(\frac{\Delta\epsilon}{\epsilon}\right)^2}$$

Also, as has been pointed out above, in order to suppress multiple scattering thin samples are necessary, and this is at the expense of scattered intensity. Consequently, another requirement for the diffraction unit is that it have a high intensity source and that it produce a high intensity-to-background ratio.

The need for high-intensity leaves out of consideration the simplest approach of using pinhole collimation. Four other types of geometries for diffraction units have been investigated and are described below.

1. Straight-Slit Geometry

Many workers have and still do use slit geometry in their diffraction units as a compromise with angular resolution in order to obtain higher intensities. Yudowitch[21] has worked out the conditions for optimum slit geometries. For two-slit systems he finds that the sample-to-film distance should equal the sample-to-source distance; that the area of the source slit should be twice that of the sample slit; and that the optimum slit height to slit width ratio depends upon the angle of scattering. Monochromatization in the two-slit systems is usually by means of filters. Guinier[1] has used a curved crystal to obtain a monochromatic beam which is of slit dimensions at the film position. DuMond[22] was one of the first to suggest the use of the double-crystal spectrometer for the attainment of high monochromatization. This was the first method of low-angle diffraction which was investigated in the work described here.

A photograph and a schematic drawing of the double-crystal spectrometer arrangement for low-angle diffraction is shown in Fig. 5. The crystals of the double spectrometer which should be of high quality are set in the position usually used for study of the "parallel-position rocking curve" of the crystals. With the sample whose low angle diffraction is to be studied placed in the x-ray beam between the two crystals the low angle diffraction results in an observable broadening of the rocking curve. Initially, an ion chamber method of detection was used, but later a superior method using a xenon-filled

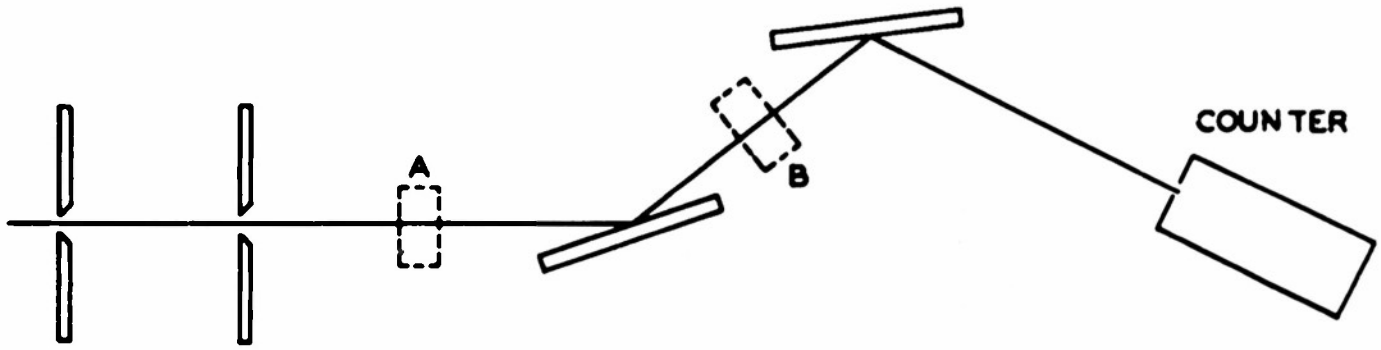

Fig. 5 Double-Crystal Spectrometer Unit

Geiger tube, especially designed and built by William West*, was employed. Preliminary work on the measurement of carbon blacks was done, using both Mo-K (0.709 A) and Cu-K (1.54 A) radiation.

This approach to low-angle diffraction measurement presents two major problems: First, it was discovered that the scattered intensity was often not much larger than that associated with the diffraction wings of the crystal rocking curve in the absence of the sample. And second, there remained the basic problem characteristic of all slit geometries which is that of correcting for the finite slit dimensions. There is of course no slit collimation per se in this double crystal spectrometer but the angular collimation resulting from the geometry of this double crystal arrangement introduces the same type of distortion and calls for the same kinds of very complicated correction to the diffraction pattern as are encountered in the case of slits.

(A) Background Subtraction Method

A background subtraction method was used successfully with the double-crystal spectrometer to overcome the first problem by taking the difference between two readings taken for each angle of scattering measured - one with the sample at position A, and the other with it at

---

* William West initiated the work in low-angle diffraction using the double-crystal spectrometer. He left this to complete a thesis on the measurement of crystal reflection coefficients, but has published later work on the low-angle diffraction measurement of clay particles. (Ref. 23)

B. Let $W(\epsilon)$ be a normalized window-curve distribution for the two-crystal spectrometer, i.e., the rocking curve in the absence of the sample. The intensity measured then at position A is

$$I_A(\epsilon) = I_o\, e^{-\mu t m^m}\, W(\epsilon)$$

And the intensity at B is very nearly

$$I_B = I_o\, e^{-\mu t m^m}\, W(0)\, \phi(\epsilon) + I_o\, e^{-\mu t m^m} W(\epsilon)$$

in which $\phi(\epsilon)$ is the diffraction scattering distribution for the two-slit system. Taking the difference $I_B - I_A$ we obtain this component of the scattering with the background subtracted out.

(B) A Method for Correcting for Finite or Infinite Slit Systems

As one may readily see from Fig. 6-a, the scattered intensity measured at a given distance from a straight-slit system is the integrated effect of contributions from a range of scattering angles, $-\theta_o$ to $+\theta_o$. Two typical cases are illustrated: (1) The detector or microphotometer window slit height is small compared with the beam height. (2) The detector of microphotometer slit height is long compared with the dimensions of the diffraction pattern. For either case the experimentally measured intensity distribution is given by the integral

$$I_x(\epsilon) = \int_{-\theta_o}^{\theta_o} I\left(\sqrt{\epsilon^2 + \theta^2}\right) d\theta \qquad (26)$$

in which I is the desired function, i.e., the intensity distribution

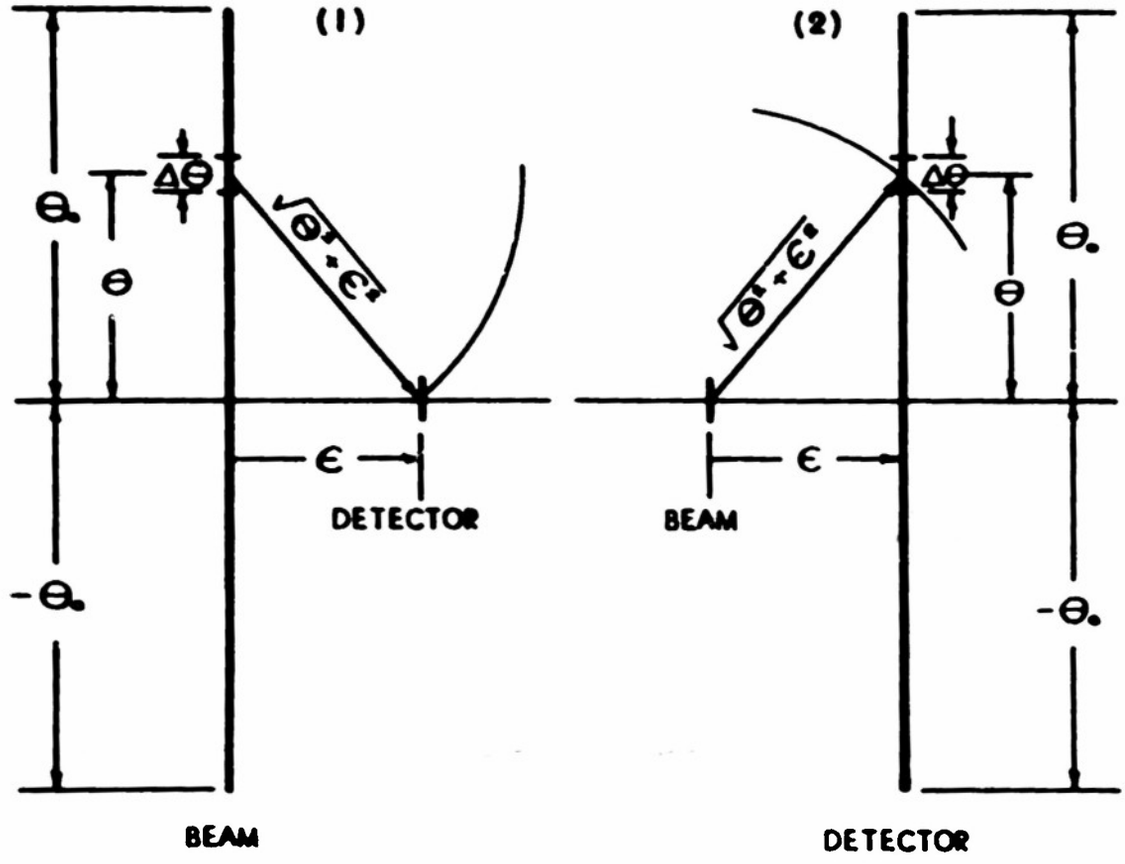

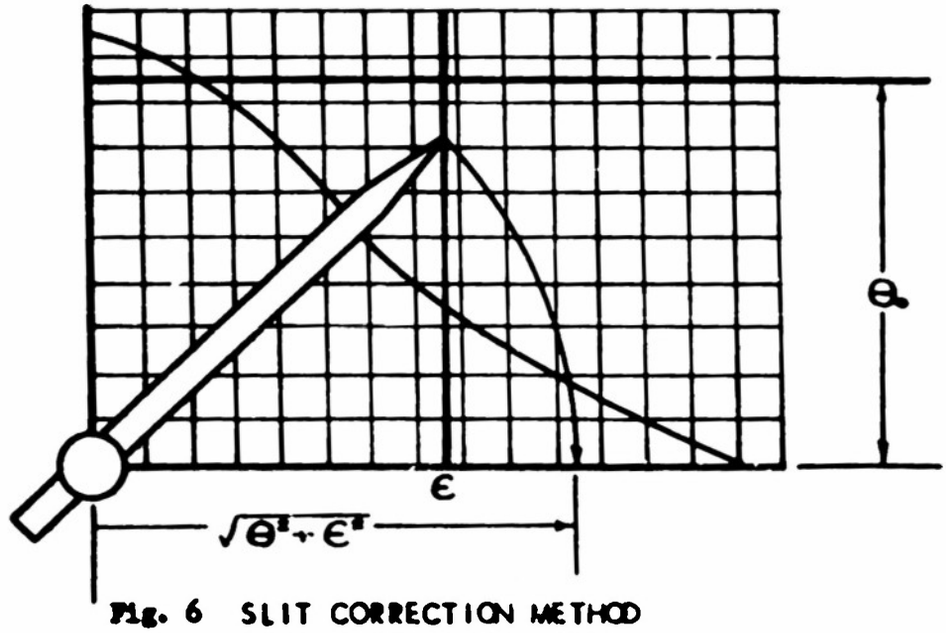

Fig. 6 SLIT CORRECTION METHOD

function for a parallel, monochromatic beam of negligible cross section.

Now suppose that ln I_x is plotted as a function of ϵ^2. At least for large angles this plot is almost invariably a straight line. In fact, as will soon be evident, if the sample were made up of spherical particles of uniform size, the entire plot would be a straight line. But say for $\epsilon > \epsilon_o$, we may write

$$I_x = A\, e^{-b\epsilon^2} \tag{27}$$

This means that for $\epsilon > \epsilon_o$ the desired, "unfolded", intensity distribution must be Gaussian also because the above integral, (26), folds a Gaussian function into another Gaussian of the same argument. This is why the measured intensity would be plotted as a straight line on the ln I_x vs ϵ^2 graph for all angles if the sample were a uniform random distribution of spherical particles, and therefore, according to the Guinier approximation, would yield a Gaussian intensity distribution

$$I = I_o\, e^{-(4\pi^2 R^2/5\lambda^2)\epsilon^2}$$

For this "ideal" sample, the measured intensity becomes a Gaussian of the same argument by (26), and the slope of the ln I_x vs ϵ^2 graph is then equal to $4\pi^2 R^2/5$ from which R is determined.

But because of non-uniformity of sizes of particles, or because of non-spherical shapes of particles, this Guinier approximation usually does not apply, and the effect of the finite slit system is to produce a measured intensity function that is of different form from that which would be due to a beam of negligible cross section. Nevertheless, it is characteristic of low-angle diffraction patterns of a

more or less non-uniformity of particle sizes to form a straight line on a ln I_x vs ϵ^2 plot for an appreciable range of angles greater than a particular angle, say ϵ_o. Thus we may obtain (26). Since the scattered distribution of intensities is not changed in form by the finite slit-system in this range of angles, let us consider this "tail" of the curve, for I_x, for which $\epsilon > \epsilon_o$, as the corrected curve, and, by a numerical integration process, extend this corrected curve into the region of smaller angles of scattering. We must then consider the resulting "folded" intensity curve as identical in form to the original curve, I_x, but multiplied by a factor F. This factor is determined by applying (22) to the portion of the curve, I_x, which is to represent the corrected curve, i.e., for $\epsilon > \epsilon_o$. Thus

$$FI_x = \int_{-\theta_o}^{\theta_o} A\, e^{-b(\epsilon^2 + \theta^2)}\, d\theta = \sqrt{\frac{2\pi}{b}}\ \text{erf}\,(b\,\theta_o)\, A\, e^{-b\epsilon^2}$$

and we obtain

$$F = \sqrt{\frac{2\pi}{b}}\ \text{erf}\,(b\,\theta_o) \qquad (28)$$

Now for the angular region less than θ_o, we may write

$$FI_x(\epsilon) = 2\int_o^{\theta_o} I\left(\sqrt{\epsilon^2 + \theta^2}\right) d\theta = 2\Delta\theta \sum_o^N I\left(\sqrt{\epsilon^2 + (n\ \theta)^2}\right)$$

where the number N is defined by the equation $(N + \frac{1}{2})\Delta\theta = \theta_o$. Now by solving for the desired intensity term, $I(\epsilon)$, which incidentally, is usually the largest term of the series in the summation, we obtain

$$I(\epsilon) = \frac{F\, I_x(\epsilon)}{2\,\Delta\theta} - \sum_{1}^{N} I\left(\sqrt{\epsilon^2 + (n\,\Delta\theta)^2}\right) \qquad (29)$$

In this way, the corrected intensity distribution for any angular position, ϵ , is determined by the measured intensity distribution at this angle and by a correction term which consists of a sum of terms based on the measured intensity for larger angles. This equation, therefore, permits a continuation of the corrected curve into the smaller angle region.

A simple method for rapidly evaluating the correction term is indicated in Feg. 6-b. Let ϵ be the angular position to which the corrected intensity curve is to be continued next. The vertical line at this angle is marked off into N divisions such that $(N+\frac{1}{2})\Delta\theta = \theta_o$, the half-angular height of the effective slit. A sliding radius arm, pivoted about the origin of the intensity curve, may then be extended to the nth division, say, so that its length becomes $\sqrt{\epsilon^2 + (n\Delta\theta)^2}$ in the angular units of the graph. The radius arm may then be rotated down to the ϵ-axis, and the term $I\left(\sqrt{\epsilon^2 + (n\,\Delta\theta)^2}\right)$ may be read off the curve. These terms may be subtracted, by machine, from the value $\frac{F\, I_x(\epsilon)}{2\,\Delta\theta}$, thus obtaining the corrected $I(\epsilon)$ according to (29).

With the methods described above of subtracting out the "wings" of the rocking curve and of correcting for the slit type geometry, it was possible to successfully use the double-crystal spectrometer for low-angle diffraction measurements. A double-crystal spectrometer has been developed by Shaw[24] for use with the long x-ray wavelengths. His instrument employs a beryl crystal of 8.06 A spacing, and a

specially designed electron multiplier tube for detection. The reflectivity of the beryl crystal for 8.56 A was measured[25], and was found to be only three percent.

Such a reduced intensity would require relatively long slits, i.e., a large θ_o. This, in turn, would demand a slit correction, as described above, which becomes less accurate as θ_o becomes large. Therefore, it would seem that the reduction in intensity and/or the loss of angular resolution associated with the use of the double-crystal spectrometer is too great to justify the gain of the high degree of monochromatization. In fact, since the intensity of the main beam in a diffraction unit is reduced just as rapidly for either a gain of angular resolution or of monochromatization, one would expect an optimum, useful intensity when the angular resolution error, $\frac{\Delta\epsilon}{\epsilon}$, and the monochromatization error, $\frac{\Delta\lambda}{\lambda}$, are approximately equal.

2. Annular Slit Geometry

A slit system of comparable "light-gathering power" to that of the two-slit system described above, but one which permits a counter measurement which does not require the above described correction for finite slit height is sketched in Fig. 7. In this arrangement the two slits consist of a pinhole and an annular slit. The pinhole may be at the source and the sample upon an annular slit as shown in (A), or the inverse arrangement may be used as in (B).

In either case it is evident that the radiation that passes through the pinhole at the counter window is characteristic of only one scattering angle. The diffraction pattern is to be explored by moving the

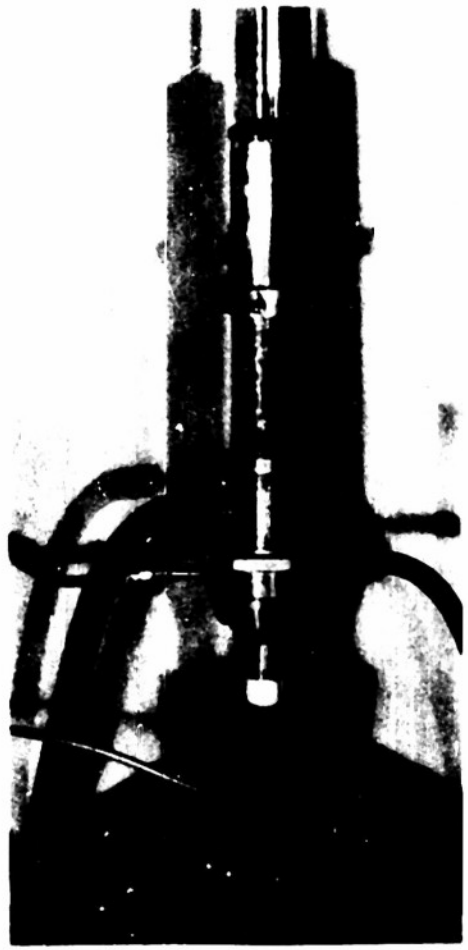

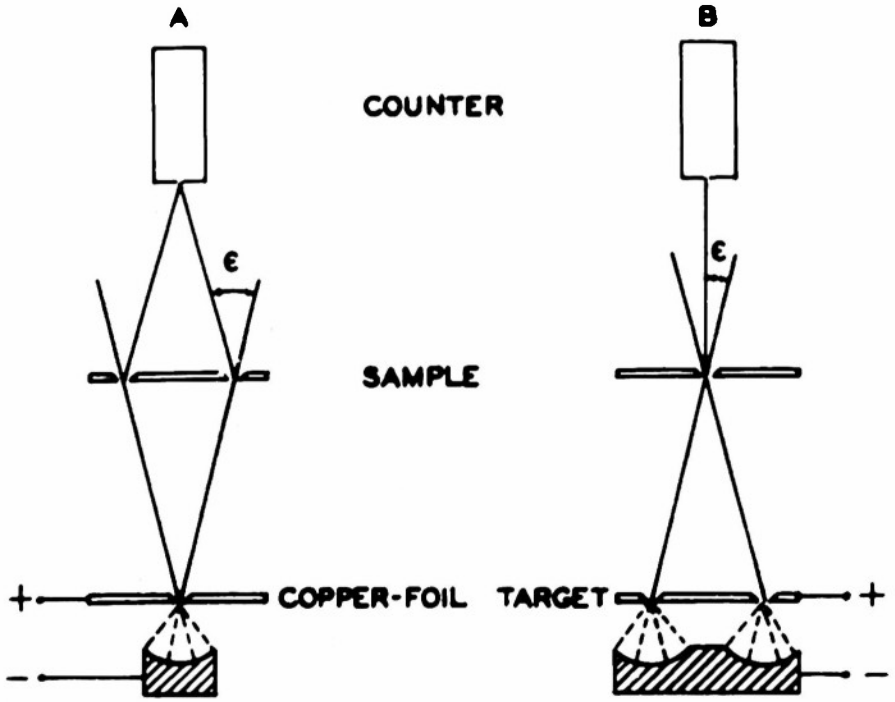

Fig. 7 Annular-Slit Diffraction Unit.

counter and its pinhole axially. The intensity gain over comparable pinhole geometries is equal to the ratio of the area of the annular slit to the area of the pinhole. An inverse-square law correction is necessary since the distance of the detector from the source is changed for each measurement of $I(\epsilon)$. However, since the low intensity at the larger angles of scattering is, in this way, increased by the inverse-square effect, this turns out to be quite favorable.

Two cameras have been constructed*, one for each arrangement, and a photograph is shown of the (B) camera. A simple gas x-ray tube was used which utilized a water-cooled transmission-type copper foil target. The Cu-L (13.3 A) line was used and the continuous radiation was minimized by using the forward direction of radiation, and by the filter action of the copper foil itself. In the (A) arrangement, the sample was fixed In the (B) arrangement, the sample was mounted on a pinhole assembly fixed onto the counter and about 5 cm. from the counter window. The counter moved in and out of an evacuated brass tube, using an "O" ring seal.

This method was successfully used to measure the same carbon blacks which were used in the double-crystal spectrometer work. The simplicity of construction and the high angular resolution which is possible with this type of geometry invited further work, but it was felt that neither the monochromatization nor the intensity obtained was

---

* K. L. Yudowitch has independently developed this approach, and has published his work in J. Opt. Soc. Am. 43, 50 (1953). The work described above was done by the writer in 1950, but was not published.

satisfactory enough.

3. Concave Mica Point-Focusing Monochromator

In order to obtain a high degree of monochromatization and to form a radially symmetric diffraction pattern which does not require any slit correction, and still maintain a workable intensity, a point-focusing monochromator would be required. Two methods seemed feasible and have been first described by DuMond[26]. The first method consists of using two bent crystals in tandem, the first forming a line focus which is reduced to a point focus by the second crystal. This instrument was designed for Cu (1.54 A) and has been described by Shenfil, Danielson, and DuMond[27,28].

The second method utilizes a single, flexible crystal such as mica. A single crystal bent with a radius, R_1, will form a line image of a point source providing that each is positioned on a circle of diameter R_1 which is tangent to the crystal, and providing that the angle θ (Fig. 8) is that Bragg angle for the radiation used. Now if a second curvature is imposed upon the crystal about an axis which passes through the source and the two focal points S and I on the circle, hence of radius R_2, the line image is reduced to a point image.

This method of achieving a point focus for x-rays is particularly appropriate for long wavelengths. One of the very few crystals which will permit enough double curvature to be effective is mica, which has a "rich" cleavage plane of spacing 9.9 A. This spacing is very nearly ideal for the long wavelength region of 10 to 18 A. Because of the softness of the crystals, because of its micro-irregularities[24], and

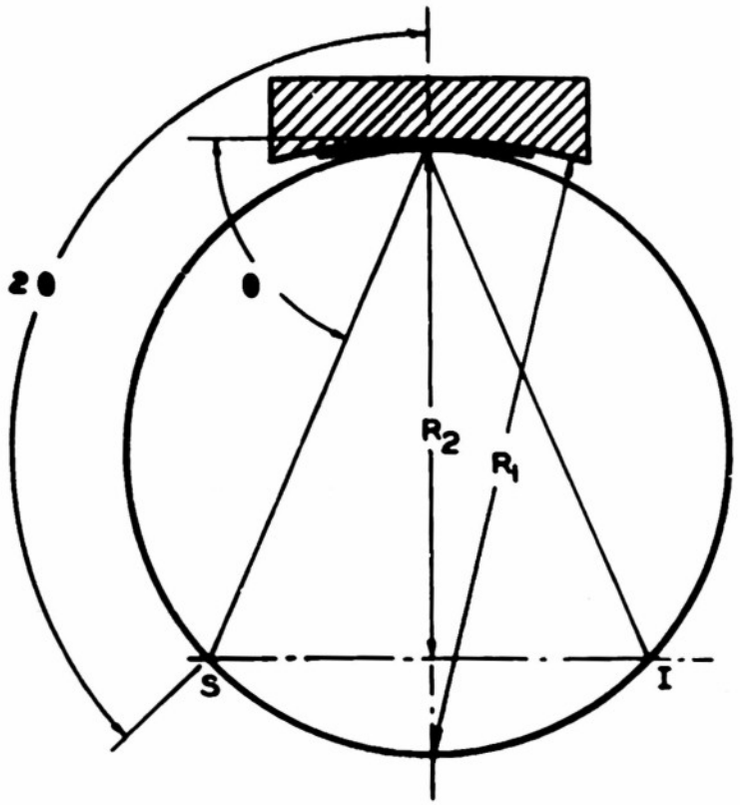

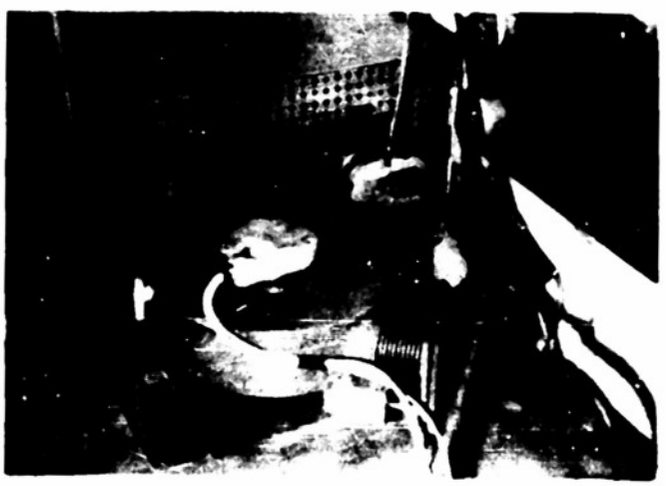

Fig. 8 Concave Mica Diffraction Unit

because of the stressing necessary to create a double curvature, it would not be expected that this type of monochromator would have a very high wavelength resolution. This, however, as discussed below, is not such a serious disadvantage for long wavelengths because of the relatively simple structure of these lines. The monochromator which was constructed was designed for the F-K (18.3 A) line, which is the only line other than relatively weak satellites in the K series of this element. For this radiation, the Bragg angle is 67 1/2° so that nearly back-reflection is accomplished with the resultant high intensity. Finally, the broadening of the focal spot due to the micro-irregularities of the crystal is not as serious for long wavelengths because of the correspondingly larger angles of scattering.

The double curvature was obtained by cementing a .005" thickness mica sheet onto a forming block of the proper double curvature under one atmosphere of air pressure. A thin layer of polymerizing cement was used with which a bubble-free, near-contact with the forming surface was obtained.

The forming block was cut from a large, cast aluminum toroid 1" thick, 2 1/2" wide, and with an inside radius of 10.459" = R_2 to the center, and with a second radius of curvature of 12.310" = R_1.

A gas x-ray tube was used with a Mg F_2 evaporated film on a water-cooled aluminum anode as target. The vacuum system was common to both camera and tube. A photograph of this diffraction unit is shown in Fig. 8.

Enough 18.3 A wavelength intensity was obtained to light a fluorescent screen (Patterson-D) faintly at the focus. However, short

exposure photographs of the focal spot were no smaller than 1.5 mm in diameter. This is five to ten times too large for good diffraction geometry. Several reasons for this broadening are suggested. The forming block was not lapped, and so was probably not very accurate. The mica tended to cleave away from the surface in small areas. And finally, the inherent micro-irregularities in the mica crystal would tend to cause a diffraction broadening of the beam.

Nevertheless, this method seemed to demonstrate greater promise than the previous two methods described above for the long wavelength region. The writer intends to work further with the problem of making suitable concave mica surfaces.

4. Total-Reflection Point-Focusing Geometry

With a crystal or grating monochromator, a considerable amount of intensity is rejected in order to secure resolving power. But for the long wavelengths of interest here, such resolving power is not necessary. In fact, the major problem in the monochromatization of these wavelengths is the suppression of the hard continuous radiation. This poses a new problem in x-ray diffraction in a wavelength region where practically no diffraction work has been done. This fact seems to invite a search for new methods.

The fourth method of obtaining a low-angle diffraction pattern with long wavelengths is based upon the total-reflection of an x-ray beam to obtain a point focus, and the utilization of the critical angle for reflection to provide an effective "cut-off" for the hard component of the continuous background radiation. High intensity point-focusing

is achieved, and an effective monochromatization is obtained without rejecting any desired radiation, in a manner very superior to straight filter methods.

A nearly cylindrical, totally reflecting mirror is used which forms a point focused image of a point source. (Fig. 9) The mirror is ground and polished into an ellipsoidal section from pyrex. A solid angle of radiation is used which is from one hundred to several thousand times that of comparable pinhole geometries.

A combination of methods has been used to suppress almost completely all background radiation. A specially designed gas-filled x-ray tube has been developed to give a high intensity of radiation in a direction 180° from that of the electron beam by placing the entrance pinhole inside the cathods focusing cup. Soft continuous radiation in this "back" direction should be a minimum. Next, the mirror is constructed so as to present angles of reflection only at the critical angle for the desired radiation. In this way, all radiation that is harder is effectively cut-off. And finally, the soft component of the background that remains is rapidly absorbed by the filter action of an appropriately chosen substrate on which the sample is mounted.

Because this method has never been explored - yet seemed very promising, and because very little work has been done with total-reflection of x-rays, it was decided to develop this approach in detail. This work will be described in the next section.

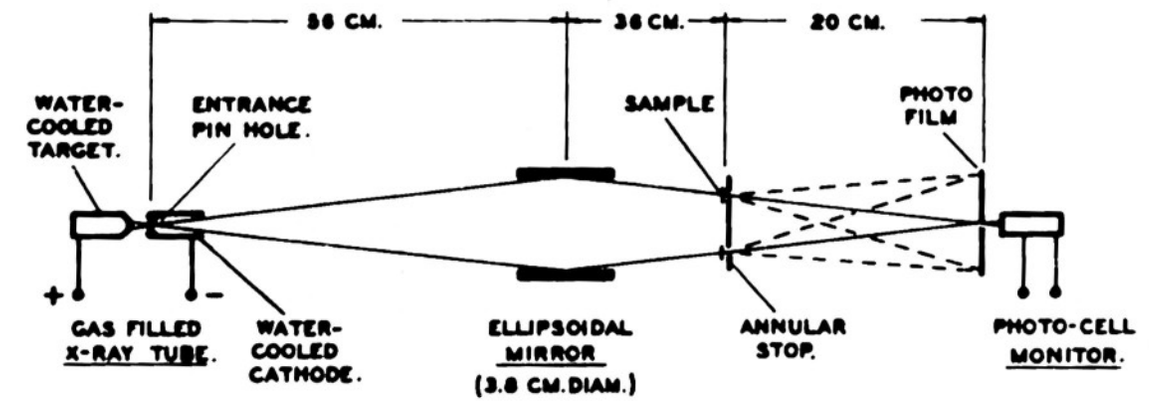

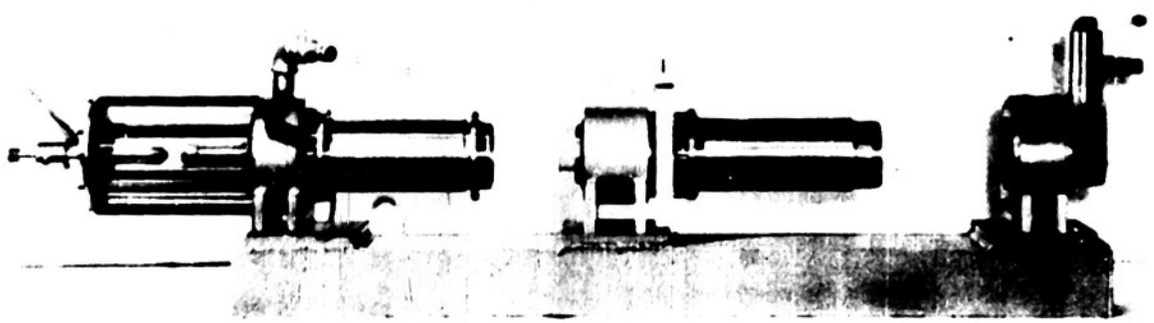

Fig. 9 Total-Reflection Diffraction Unit

IV. DESIGN AND CONSTRUCTION OF THE TOTAL-REFLECTION UNIT

1. Monochromatic Long-Wavelength Sources

A survey of the long wavelength lines will show that there are several which are very sharp and are completely dominant over the other lines in their series, and over their satellite structure, Gwinner[29] has made a detailed study of the L-series lines from Ge-L (10.42 A) to Fe-L (17.57 A). Of these, the Ni-$L_{\alpha_{1,2}}$ line is outstandingly sharp and free of satellite structure. It is very strong compared with the β_1 line, which is only two percent harder. (Ni-$L_{\alpha_{1,2}}$ = 14.53 A and Ni-L_{β_1} = 14.25 A). The full line-width at the half-maximum point is 2.2 10^{-4} A.U. or 1.5 10^{-3} percent of the wavelength. It is of interest to compare these values with corresponding ones for the ordinary wavelengths. The β_1 line of Cu is 20 percent as strong as the α_1 line, and the difference in wavelength is 10 percent (Cu-K_{α_1} = 1.54 A, Cu-K_{β_1} = 1.38 A). The width of the $K_{\alpha_{1,2}}$ doublet is .26 percent of its wavelength.

Of the long wavelength K series lines, O-K (23.6 A) is very strong compared with any associated background[30]. Its line breadth is somewhat less than 1 A.U., or about four percent of the wavelength. The K series lines seem considerably stronger than comparable wavelengths in the L series, but are characteristically broader.

The Cu-L_{β_1} is of appreciable intensity compared with the Cu-$L_{\alpha_{1,2}}$, and cannot be neglected. However, the combination Cu-$L_{\alpha,\beta}$ is a strong and easy radiation to produce, and has been very convenient to use for exploratory work. The effective width of the combination

Cu-$L_{\alpha,\beta}$ radiation is still less than three percent of the wavelength.

Another radiation, Al-K, has been used and has certain special advantages. (1) For very small particles, 20 to 200 A.U. in size, this shorter wavelength of 8.32 A.U. would give the more favorable λ/R ratio. (2) The Al-K radiation is very strong, and the aluminum target is durable and easy to cool so that a relatively large amount of power can be used in the x-ray tube. (3) The small amount of aluminum that is sputtered onto the anode from the aluminum cathode focusing cup cannot, of course, "contaminate" the anode. (4) The best filter for aluminum radiation is aluminum foil which is easy to obtain and to handle, even in very thin leaf form.

However, this long wavelength radiation has also a particular disadvantage in that its $K_{\beta 1}$ (7.97 A) radiation is not of negligible intensity, and is five percent harder. Aluminum filtered K-series Al radiation would not have sufficient monochromatization for precise low-angle diffraction work. The writer proposes the following method for reducing this β_1-radiation of Al-K radiation but wishes to point out that only preliminary work has been done on this method, to date.

In Fig. 10-a, the curve showing the variation of θ_c with wavelength near a critical K-absorption edge of an aluminized reflector is plotted. This was obtained from the equation for θ_c, $\theta_c = \sqrt{2\delta}$, in which δ is obtained from the quantum-mechanical expression derived by Hönl[31]. It is noted that at the critical absorption wavelength, there is a very abrupt decrease in the critical angle of reflection. This has been observed experimentally[32]. Since the

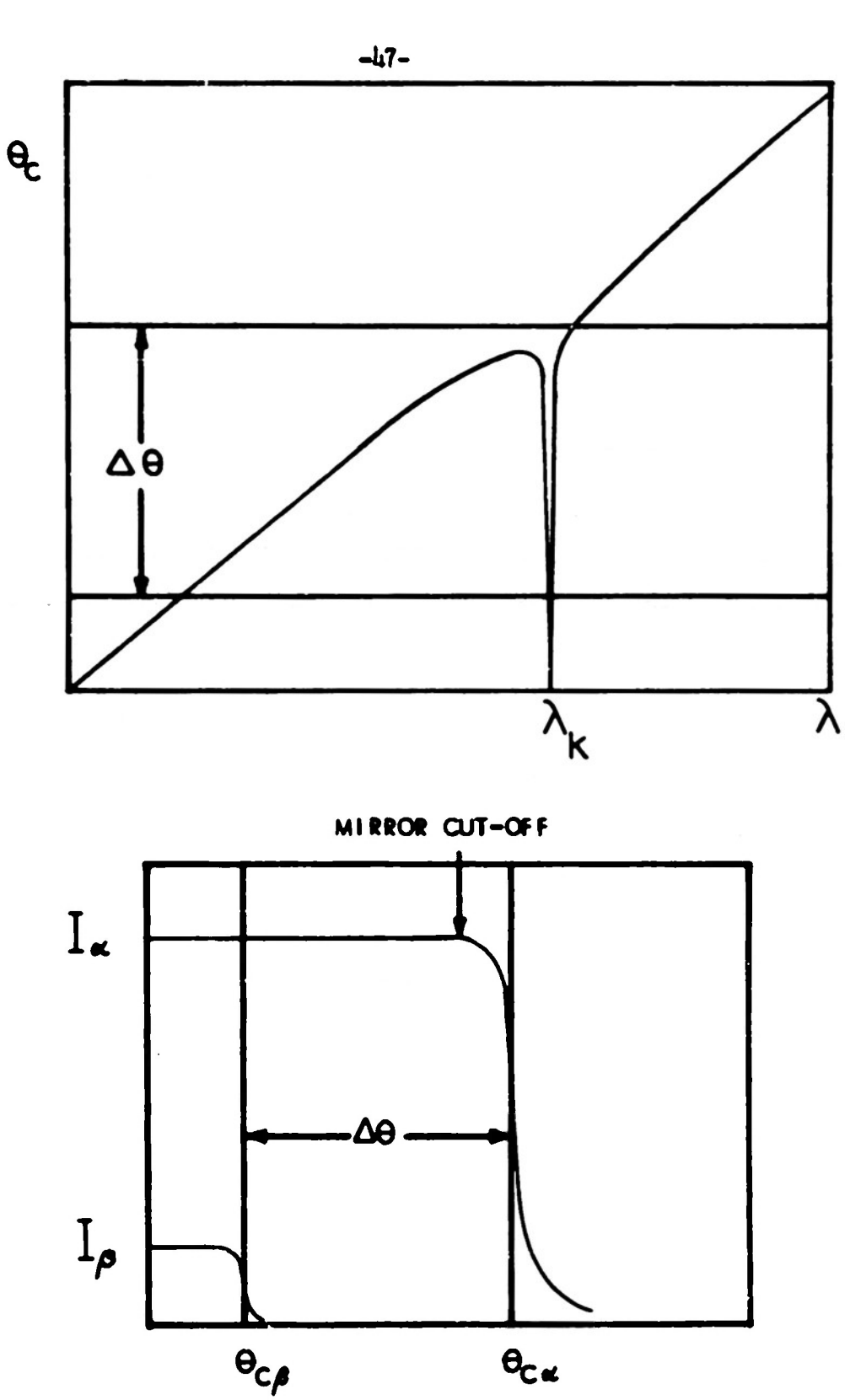

Fig. 10 SUPPRESSION OF AL-K_β RADIATION

Al-K_{β_1} (7.965 A) and the Al-$K_{\alpha_{1,2}}$(8.320 A) lines are .4 percent and five percent longer in wavelength than the critical absorption wavelength, 7.936 A.U. respectively, it would be expected that there would be an appreciable difference in the critical angle of reflection for these two lines. Therefore, by constructing the aluminized ellipsoidal mirror of such diameter as to present effectively only the critical angle of reflection for the $K_{\alpha_{1,2}}$ line, the K_{β_1} line should be appreciably reduced in intensity since this angle of reflection is not favorable for this harder radiation. See Fig. 10-b. It would seem that this method should yield a very high intensity of Al-$K_{\alpha_{1,2}}$ (8.32 A) radiation, which would be much more monochromatic than would be possible with the filter technique alone.

Another favorable aspect of long wavelength monochromatisation is that the ratio of the intensity of the characteristic radiation to that of the associated continuous background radiation increases very rapidly with wavelength(33). Also, it has been observed(33) that this ratio increases with the voltage. This latter fact may have been deduced from the well known observations that the characteristic intensity increases with $(V-V_o)^{1.7}$ and the continuous radiation in the region of the characteristic radiation increases with $(V-V_o)$. Therefore, for high voltages relative to the line excitation voltage, V_o, the ratio of characteristic to continuous radiation increases approximately with $V^{.7}$. Consequently, since no crystal monochromator is used, and there is therefore no danger of passing second-order radiation, it is possible to further emphasize the characteristic radiation over the continuous radiation by running the x-ray tube at higher than usual voltages,

utilising the "cut-off" of the mirror to eliminate the resulting hard component of the continuous radiation. In this way, increased efficiency of x-ray production, hence higher intensities, may also be obtained by virtue of the higher tube voltage.

For the O-K (23.6 A) line, SiO_2, Al_2O_3, and BeO targets were used. These were obtained (1) by imbedding a thin quartz disk into a water-cooled anode of copper, (2) by "anodising" the tip of an aluminum anode, and (3) by painting an acidulated solution of BeO onto the tip of an anode, respectively. Oxygen targets made by the first two methods were or relatively high efficiency because of the effect of secondary production from the Si and Al atoms. With these targets, the usual leveling-off of the intensity versus voltage curve was not reached for the same reason. The anodised surface was the easiest to cool, and, therefore, to maintain.

In spite of the fact that the oxides used for target material were refractory, they would decompose under the high-intensity bombardment of the electron beam in a matter of a few hours. Because of the rather effective water-cooling of the anodes, very little deterioration of the Al, Ni, and Cu metal targets has been noticed after hundreds of hours of use.

2. The Gas-Type Tube

There were several reasons for choosing a gas-filled tube for long wavelength diffraction work. (1) Its simplicity and complete demountability makes it ideal for research purposes. (2) For these wavelengths, it has been found to be very stable, and permits the

focusing of an electron beam onto the anode which is very intense. (3) This tube does not require as high a vacuum as does the filament type tube and therefore it is possible to use it "open" to the evacuated camera so as to avoid the use of thick windows.

A cross-sectional drawing of the tube is shown in Fig. 11. It will be noticed that the entrance pinhole is located in the cathode focusing cup. Therefore, only the radiation 180° from the electron beam direction is used. It is in this direction that the continuous radiation will be a minimum.

The target is indented with a cone-shaped hole at the electron beam focus. In this way, the atoms which can be "seen" by the mirror through the pinhole give off radiation not only by direct bombardment under the electron beam, but also by secondary radiation excited by the fluorescent absorption of harder components of the general radiation in the neighboring region of the hole. In extreme cases where even more radical suppression of the continuous radiation might be required, it might be relatively simple to use a similar geometry so that only this indirectly excited secondary component of the line radiation would enter the camera.

Because of its very low sputtering rate, pure aluminum is used for the focusing cathode cup. This screws into place, holding in contact with the cathode support - a thin 1/8" diameter aluminum disk, in which is drilled an .008" "pinhole".

It was found that by enclosing the exposed cathode-supporting structure with a pyrex jacket, the tube operated more "quietly", and very little sputtered material would reach the outer glass walls.

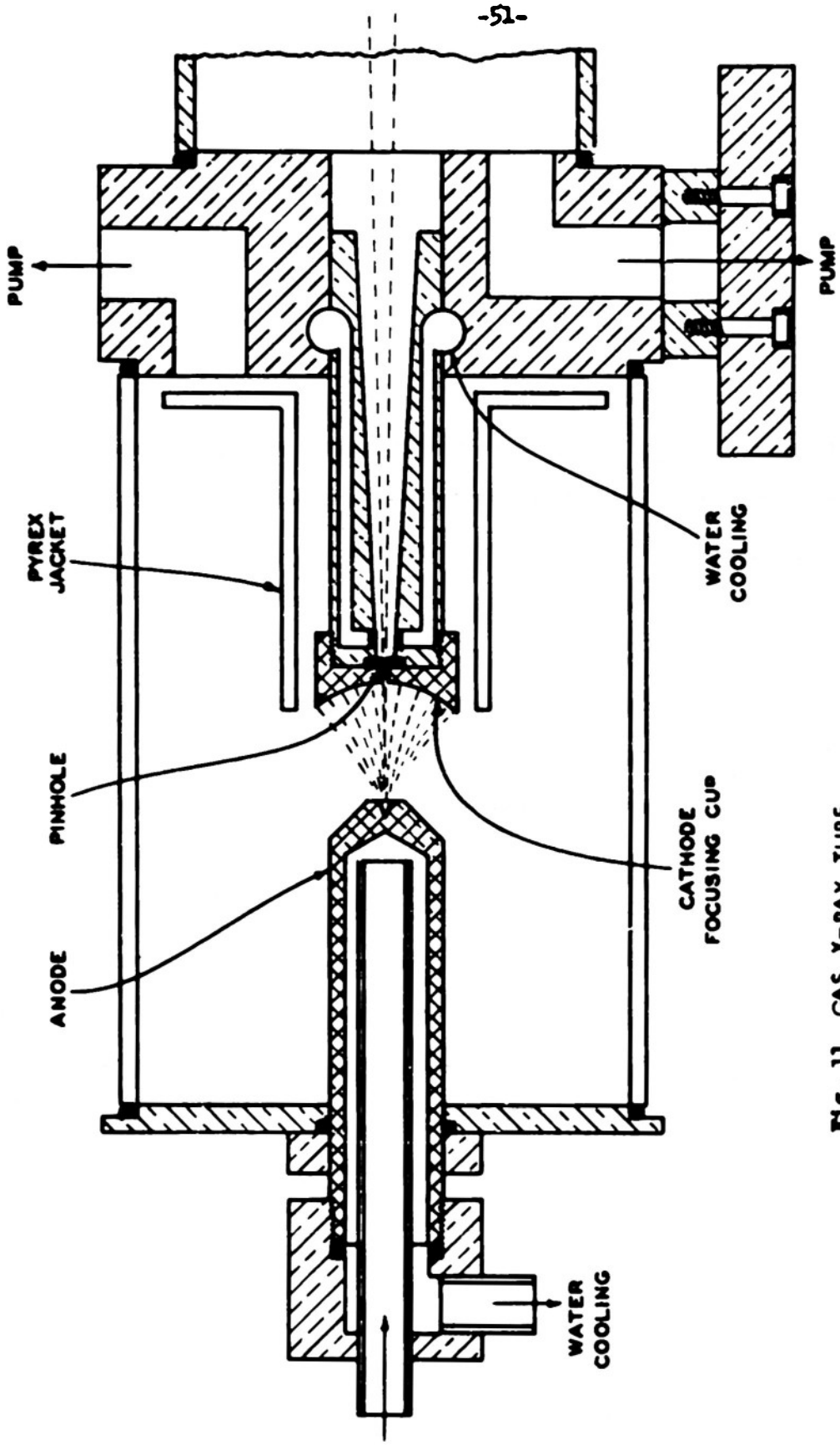

Fig. 11 GAS X-RAY TUBE

The operating limit of power for the tube has not been determined. A typical operating condition is 40 to 50 ma at 5,000 volts. The stability has been such that after about a two-hour period for stabilisation, the tube may be left for a period of days without attention.

3. The Total Reflection of X-Rays - General

A survey of the literature on total reflection of x-rays was made, and a bibliography is given in the references (34 to 55). One is impressed with the fact that relatively little work has been done on this subject, particularly since 1932.

Below is a summary of the results of the work which has been done, as described in these references, with respect to the reflection of long wavelengths.

(1) Al-K (8.32 A), Cu-L (13.3 A), and O-K (44.5 A) have been studied for total-reflection from glass, quarts, steel, silver, and gold. The reflected intensity versus angle of reflection is given for the region of angles near the critical angle.

(2) The experimental values measured for the critical angles agree only roughly with the theories of total-reflection viz., the Drude-Lorentz, the Kramers-Kahlman-Mark, and the Hönl theories. For wavelengths which are not close to an absorption edge of the reflector, the simple Drude-Lorentz expression for the critical angle is as good as any. This is

$$\theta_c = \sqrt{2\delta} = \left(\frac{n e^2}{\pi m c^2}\right)^{1/2}\lambda = 2.32 \times 10^{-3} \left(\frac{\rho Z}{M}\right)^{1/2} \lambda \qquad (30)$$

(3) The shape of the "cut-off" in the curve of reflected intensity vs angle of reflection is only roughly predicted by the Fresnel theory(56).

(4) Mohr(46) has given some approximate values for the reflection efficiencies for various surfaces for 8.3 A and 13.3 A radiations. He found 25 - 30 percent reflection for glass, 15 percent for steel, and five percent for gold reflectors. Recalling the densities of these reflectors, 2.7, 7.7, and 18.9 respectively, we note that the efficiency of reflection is approximately proportional to the reciprocal of the reflector density.

(5) Ehrenberg(54) has measured the broadening of a line image by total-reflection from a curved mirror. He attributes the effect to diffraction from Fourier components of an inherent structure of the reflecting surface.

4. A Method for the Measurement of the Critical Angle of Total Reflection

Because of the need for more information on critical angles of total-reflection than is available, it was felt that it would be advisable to devise some method for measuring these. A very simple apparatus was developed which permits a precise measurement of θ_c, and it fits easily into the diffraction camera so that no elaborate arrangement was necessary. A sketch of the geometry for this measurement is shown in Fig. 12. Filtered radiation from the pinhole in the cathode of the x-ray tube finds a uniform distribution of planes at

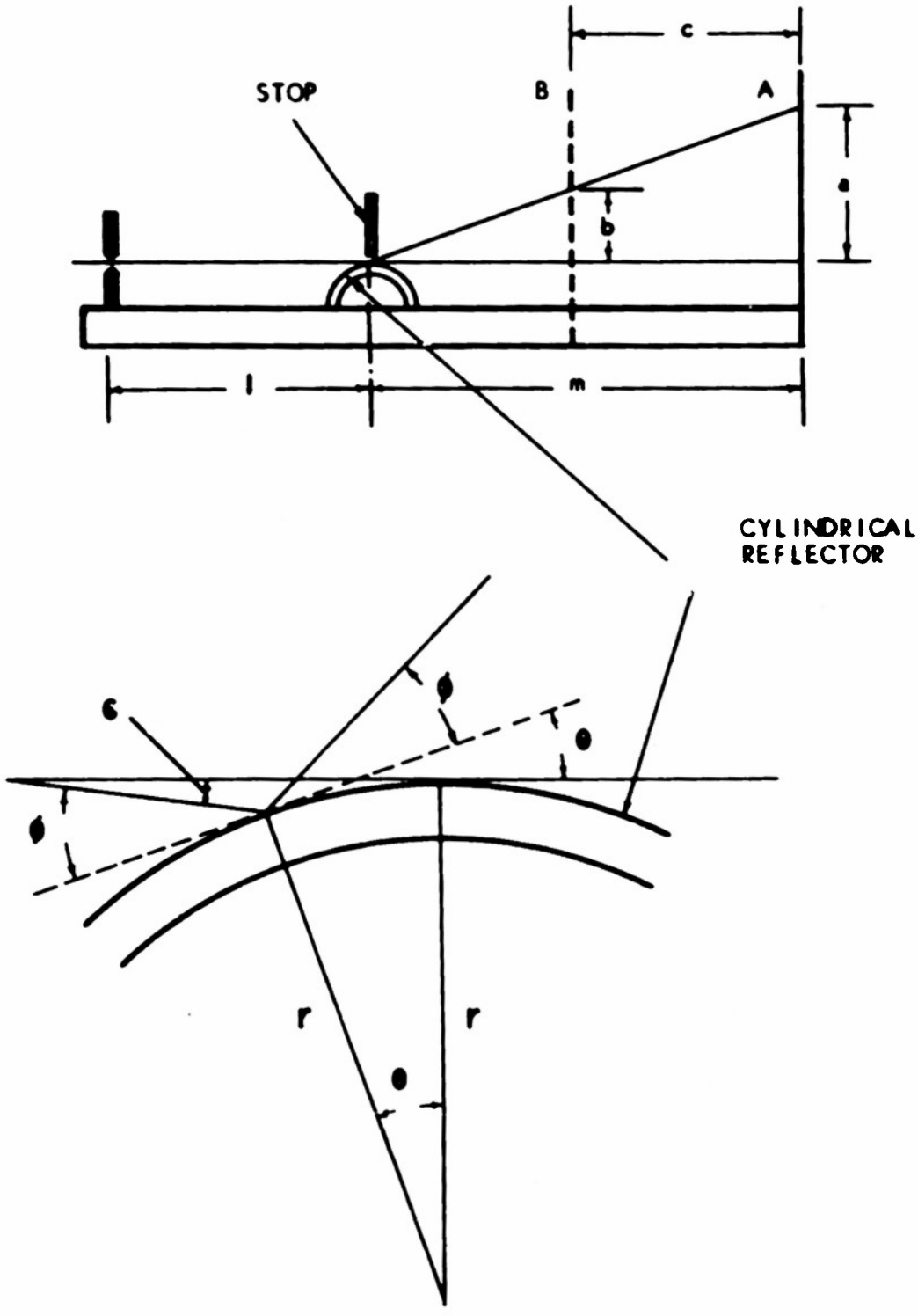

Fig. 12 MEASUREMENT OF θ_c

various angles to the incident beam on a cylindrical reflector from which it is "totally reflected" in accord with specular law over the permissible range of grazing angles up to the critical limiting angle and passes thence onto a photographic film. From the geometry, it is readily seen that

$$\phi - \theta = \epsilon = \frac{r}{l}(1 - \cos\theta)$$

Therefore, for the small angles involved

$$\epsilon = \phi - \theta = \frac{r}{2l}\theta^2 \quad , \qquad \text{and so} \qquad \phi \approx \theta$$

Now if we define I_o as the flux per unit solid angle from the pinhole source, and E_o as the flux per unit area at the film, we obtain for that flux which is included in the range ϵ to $\epsilon + d\epsilon$ and in the corresponding range $(\theta + \phi)$ to $(\theta + \phi) + (d\theta + d\phi)$

$$dF = I_o \frac{wld}{l^2} = E_o \left(\frac{m+1}{l} w\right)(m)\ (d\theta + d\phi) \quad \text{where } w = \text{width pattern.}$$

Solving for E_o we obtain

$$E_o = \frac{I_o}{2m(m+1)} \frac{d\epsilon}{d\theta} = I_o \frac{r\theta}{2ml(m+1)} = I_o \frac{I_o\, r\phi}{2ml(m+1)}$$

So finally, the flux per unit area at the film multiplied by the reflection efficiency function for the reflector, $R(\phi)$, gives us the measured distribution along the film

$$E_x(\phi) = E_o(\phi)\ R\ (\phi)$$

Hence the reflection efficiency

$$R(\phi) = \frac{ml(m+1)}{r\, I_o} \quad \frac{E_x(\phi)}{\phi} \tag{31}$$

In practice, it may not be possible to measure precisely the distance l. For this reason a second film may be exposed simultaneously to one-half of the reflected beam at position B. Since the distance between films may be measured very accurately, the critical angle may be obtained from the relation

$$\theta_c = (a - b)/c \tag{32}$$

The usual method for measuring θ_c is to intercept a slit-collimated beam of x-rays by a plane mirror which is rotated through a series of angles. At each of these an exposure of constant time duration is made on a film. There are several significant advantages of the method used here. (1) A simultaneous curve of reflected intensity is obtained for all angles, with a high resolution, and there is no dependence upon possible fluctuations of the x-ray source during an exposure. (2) The geometrical effect of obtaining an experimentally measured distribution given by the reflection efficiency function multiplied by the angle of reflection is favorable because it extends the cut-off region so that it fits more conveniently into a measurable range of photographic densities. (3) Using two film positions not only permits a more accurate measurement of θ_c, but yields two complete photographic density scales with corresponding points at a known ratio of intensities, $(m/m - c)^2$. This permits an "internal" calibration of

the film with each measurement. In fact, this same artifice has proven very useful for the calibration of the low-angle diffraction films.

Three reflection photographs taken by the method described above are shown in Fig. 13, and are as follows: (a) Aluminum filtered Al-K series radiation reflected off glass. (b) Aluminum filtered Al-K series reflected off of an aluminized surface. (c) Aluminum filtered Al-K series reflected off an evaporated nickel film on glass. (d) Aluminum filtered O-K line reflected off of glass.

(a) and (b) are taken simultaneously from a glass surface half of which was aluminized to an opaque coat. It is noticed that the calculated θ_c from the Drude-Lorents equation for δ given in (30) is in good agreement with this measurement. Since the densities of the two reflectors, glass and aluminum are the same, any effect due to the critical absorption edge for the aluminum reflector should be indicated by a smaller critical angle of reflection. As is noted here, the strong K_α (8.32 A) component of the radiation is far enough away from this edge so that very little difference in the critical angle obtains.

Again, the Drude-Lorents expression yields a θ_c for Al-K on a nickel surface (c) which is in good agreement with experiment.

This is certainly not the case for the O-K reflection off of glass (essentially Si O_2). Since the O-K (23.57 A) is so close to the critical absorption edge oxygen of 23.5 A.U., a very abrupt decrease in θ_c results.

These results are preliminary, but they do indicate several points of interest here. (1) The method described above is effective in the

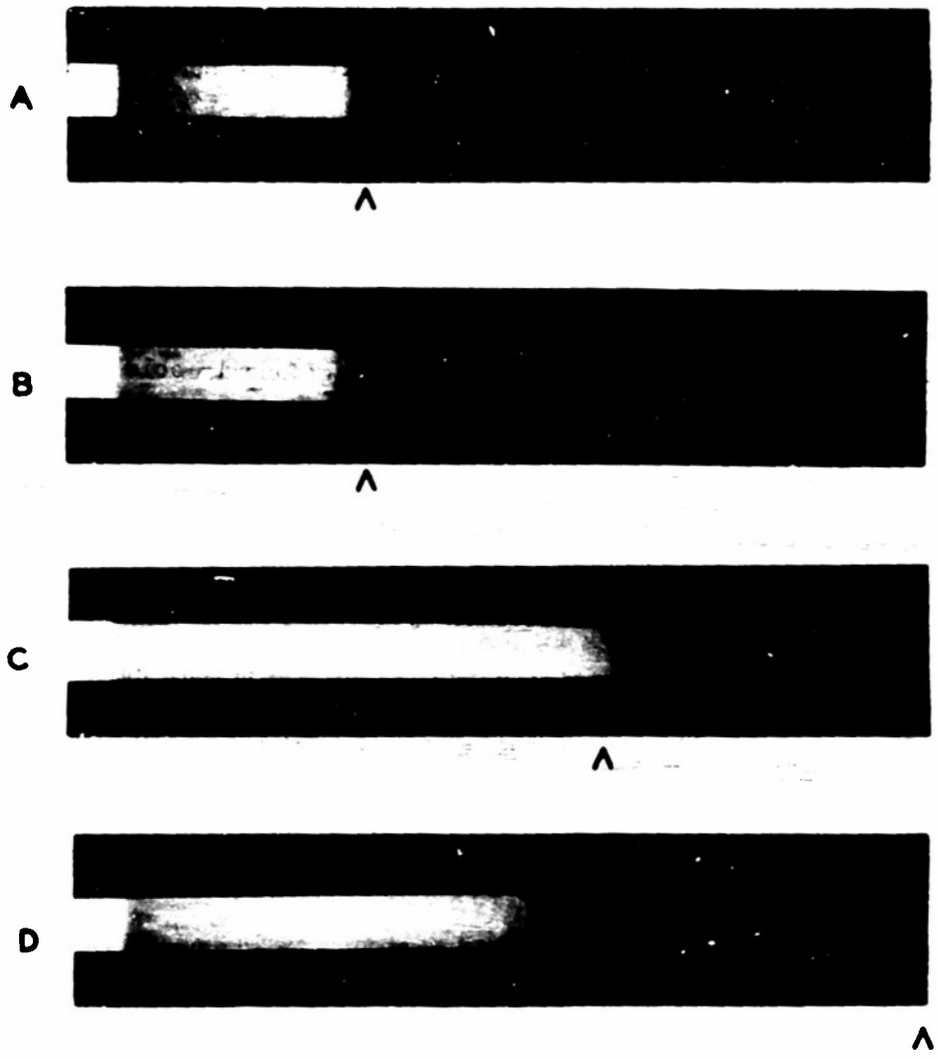

MEASUREMENT OF θ_c

RADIATION	A.U.	REFLECTOR
A	8.32	GLASS
B	8.32	ALUMINUM
C	8.32	NICKEL
D	23.6	GLASS

Fig. 13 Positions for Θ_c as calculated from the approximate Drude-Lorentz expression are indicated by the arrows.

measurement of critical angles of reflection for soft x-rays. (2) The very large change in the θ_c for the O-K line does lead one to expect the same for the Al-K_β line, thus providing effective monochromatization of the Al-K radiation by the total reflection "cut-off" technique which was described above. (3) The sharp cut-off in the reflection curve exhibited in these photographs establishes the fact that very little continuous radiation background is able to leave the x-ray tube by virtue of the 180° direction of the x-ray beam with respect to the electron beam direction, as discussed above. It should be noted that the intensities and therefore the blackening of the photographic film is to be divided by the angle of reflection in order to obtain the true reflection curve. Thus the actual cut-off of the reflection curve is considerably sharper than the cut-off which is indicated by these photographs.

5. Mirror Geometry

Ideally, the mirror should be a section of an ellipsoid of revolution with the point source of x-radiation and the point image at the respective foci. Certain geometrical properties which will be useful, and which are very easily derived are listed here (using the notation of Fig. 14). The radius of the circular arc that best approximates the ellipse at the center is given by

$$R = a^2/b \tag{33}$$

The angle of incidence, θ, of the ray reflected by the mirror at

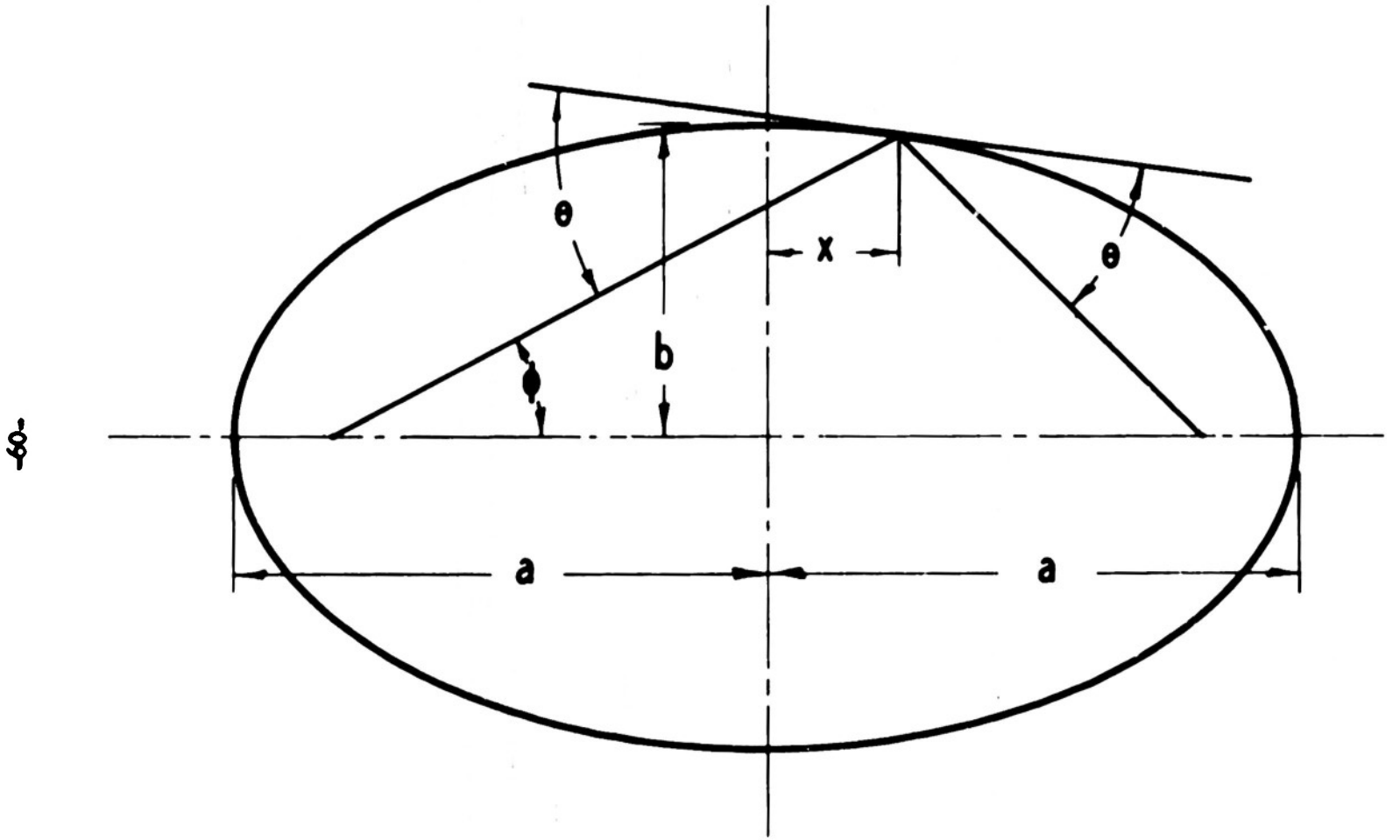

Fig. 14 ELLIPSE GEOMETRY

distance x from the center is given by

$$\theta = (b/a)\ (1 + \tfrac{1}{2}(x/a)^2 + \cdots) \tag{34}$$

The angle ϕ which this incident ray makes with the axis as it leaves the source pinhole is given by

$$\phi = (b/a)\left(1 - (x/a) \cdots\right) \tag{35}$$

The solid angle presented to the source by the mirror is given by

$$\Delta\Omega = 4\pi(b/a)^2\ (x/a) \tag{36}$$

6. Comparison to Pinhole Geometry

The gain in intensity over the pinhole geometry is the ratio of the solid angle presented to the source pinhole by the mirror to that subtended by the focal spot at a point distant 2 a away.

$$R = \frac{\left[4\pi\left(\frac{b}{a}\right)^2\ \left(\frac{L}{2a}\right)\right]}{\left[\frac{\pi r^2}{4a^2}\right]} = 8\left(\frac{b}{a}\right)^2\ \frac{aL}{r^2} \tag{37}$$

in which L is the length of the mirror. Using values for the geometry currently used, (b/a) = .034, a = 56 cm., L = 10 cm, and the radius of the focal spot r = .2 mm, we obtain a value for the gain of intensity, R = 5750. But this must be multiplied by the 30 percent reflection efficiency for glass so that the net gain is the factor 1730.

7. Aberration Equations for the Approximated Ellipsoidal Mirror

In order to learn how good the circular arc approximation is,

and to determine the effect of a deviation from the calculated radius of curvature upon the image size, an aberration equation is derived. In Fig. 15, we have let $R = R_o + \Delta R$, where $R_o = a^2/b$, from (33) is the proper radius. We then find that the radius of the circle of confusion is

$$\rho = 2\left(\frac{b}{a}\right) x \frac{\Delta R}{R} - b\left(\left(\frac{x}{a}\right)^3 + 2\ \frac{b^2\, x}{a^3}\right) \qquad (38)$$

in which the first term arises from not having the proper radius for the mirror and the second is that of spherical aberration. Using the same values as given above, with $x = 5$ cm., we obtain the size of these two errors.

$$\rho = .34\ \Delta R/R + (1.75\ 10^{-3})\ \text{cm.}$$

It is evident that the spherical aberration will be small compared to that due to a practical deviation in R. In order to limit the broadening of the focal spot to .1 mm., $\Delta R/R$ must be less than three percent error.

8. Error Due to the Finite Size of the Sample

The sample is mounted upon a thin film of metal foil or plastic which is stretched across an annular slit through which the beam passes. It may be readily shown that for the usual "small" angle scattering there is negligible error due to a finite sample size even though the film is flat. However, particularly for the long wavelengths, "medium" angle scattering might often be of interest, and the equations developed in the theory section, Part II, apply to this region as well.

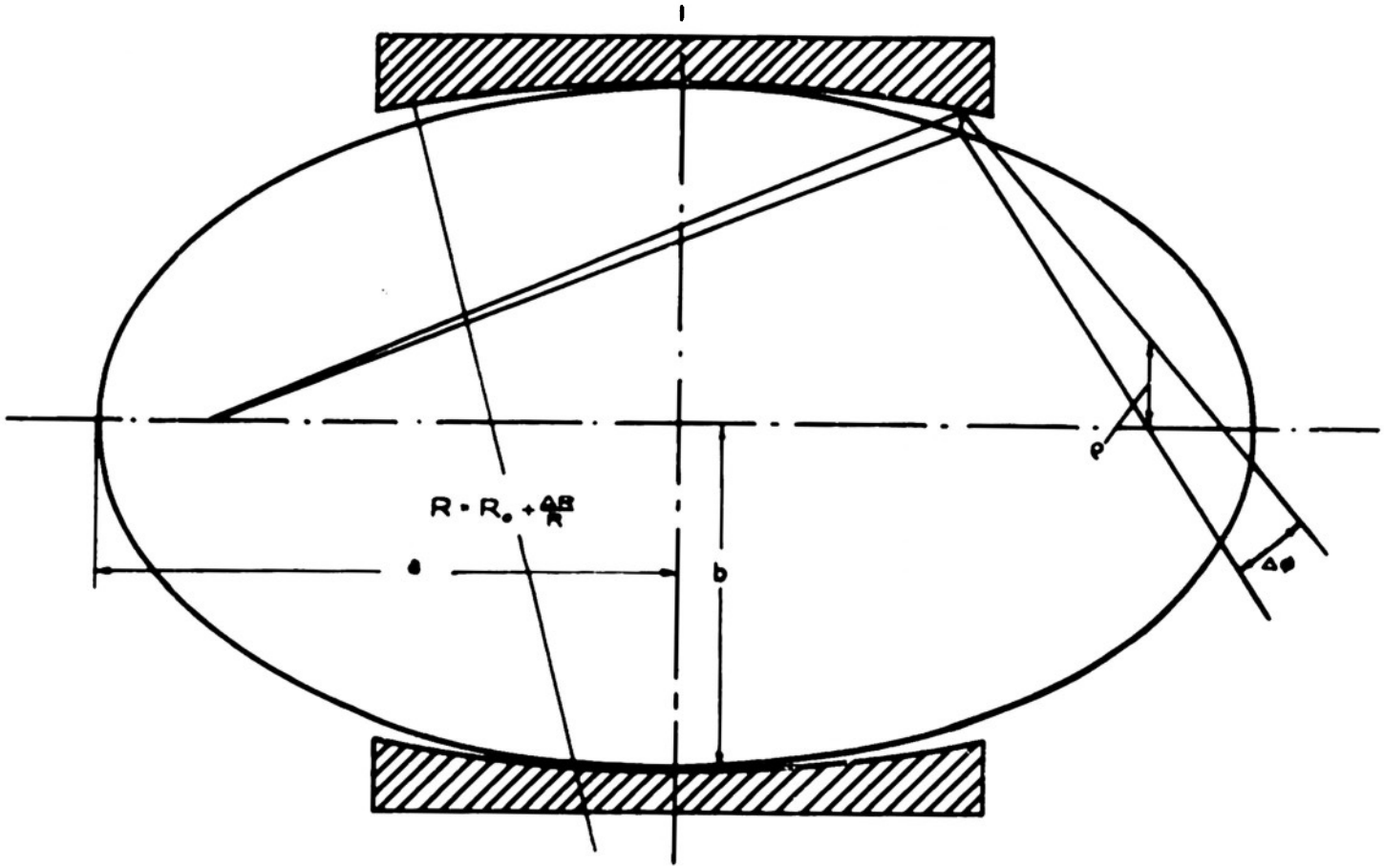

Fig. 15 ABERRATION GEOMETRY

In order, then, to focus the entire diffraction pattern without error due to the large dimensions of the sample, the film must be pressed onto a cylindrical (or spherical) form of radius equal to one-half of the distance from the sample to the film. From Fig. 16, it is seen that

$$\cos \epsilon = (a^2 + b^2 - c^2)/2ab$$

where

$$a^2 = r^2 + d^2$$

$$b^2 = r^2 + x^2 + y^2 - 2ry \cos \theta$$

$$c^2 = x^2 + y^2 + d^2 - 2dx$$

We shall now differentiate $\cos \epsilon$ with respect to θ, which derivative we shall equate to zero in order to determine the conditions under which ϵ is least sensitive to θ. We note that b, only, depends upon θ, and letting $b' = db/d\theta$, we obtain

$$(b^2 + c^2 - a^2) = 0$$

since b' is not necessarily 0; then by substituting the values above into this equation we obtain

$$x^2 + y^2 - dx = ry \cos \theta$$

Since the average value of the relatively small term, $ry \cos \theta$, is zero, we substitute this value into the above equation to obtain the condition for minimum error due to finite sample size

$$x^2 + y^2 - dx = 0$$

But this is the circle with a center at $x = d/2$.

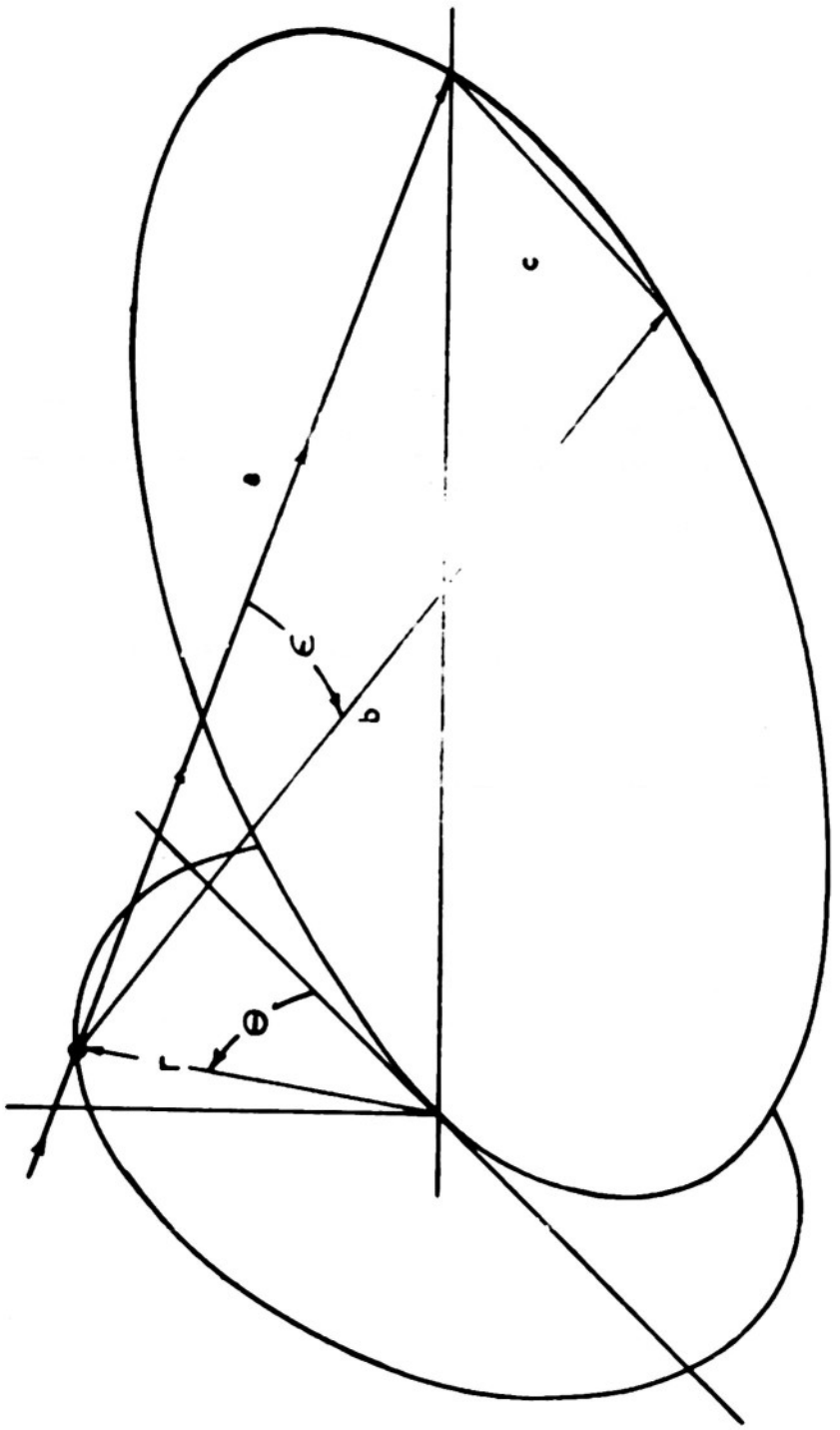

Fig. 16 Finite Sample Geometry

Now substituting this condition back into the equation for cos ϵ , we obtain

$$\cos \epsilon = \frac{(x^2 + y^2 + r^2) - ry \cos \theta}{a\left((x^2 + y^2 + r^2) - 2\, ry \cos \theta\right)^{1/2}}$$

Now let $b_o^2 = x^2 + y^2 + r^2$, and $\phi = ry \cos \theta / b_o^2$, then this may be written as

$$\cos \epsilon = \frac{b_o}{a} \frac{1 - \phi}{(1 - 2\phi)^{1/2}}$$

Expanding in powers of ϕ we obtain

$$\cos \epsilon = \frac{b_o}{a} \left(1 + \frac{1}{2}\phi^2 \cdots\right)$$

In order to determine the maximum variation in ϵ with θ, we determine the change in cos ϵ between the values for $\theta = 0$ and $\theta = 90^o$.

$$\Delta(\cos \epsilon) = -\frac{1}{2}\left(\frac{r^2 y^2}{ab_o^3}\right) = -\sin \epsilon \, \Delta \epsilon$$

Consequently

$$\frac{\Delta \epsilon}{\sin \epsilon} = \frac{1}{2 \sin^2 \epsilon} \frac{r^2}{ab_o} \left(\frac{y}{b_o}\right)^2 \approx \frac{\Delta \epsilon}{\epsilon}$$

Now letting $y/b_o = \sin \epsilon$, and $r/b_o = \sin \theta_c$, we obtain finally for the relative error, $\frac{\Delta \epsilon}{\epsilon}$ due to finite sample size.

$$\frac{\Delta \epsilon}{\epsilon} = \frac{1}{2} \sin^2 \theta_c \approx \frac{\theta_c^2}{2} \qquad (39)$$

And for the mirror of $\theta_c = .034$ $\frac{\Delta\epsilon}{\epsilon} = .06$ percent. Therefore, with a curved film, there is no appreciable error due to finite sample size even though the angles of scattering may be relatively large.

9. Choice of Mirror Material

There are two strong reasons why glass seems to be the most appropriate material with which to construct total-reflection mirrors. First, the relatively short x-ray wavelengths compared with the wavelengths of light places an even higher requirement on the smoothness of the surface. And second, the need for a very precise circular arc in the mirror cross section invites the proven, accurate methods of random optical lapping techniques, which are most highly developed for glass.

An apparent objection to using glass is that a choice of stainless steel, for example, because of its higher density, would allow a larger diameter mirror for a given wavelength, and therefore considerably higher intensities than that obtained from the corresponding glass mirror. A glass mirror, in fact, could be given an evaporated or sputterred film of some dense metal, as gold, thus permitting larger mirrors. It was found, however, that gold-evaporated films age badly in that after a few weeks the film deteriorates into a grainy surface which gives a large background diffraction pattern of its own.

Nevertheless, as was deduced above from Mohr's work[46], the reflection efficiency for total-reflection varies inversely with the density of the reflector. And from (36) we note that the solid angle presented by the mirror is proportional to $(a/b)^2 = \theta_c^2$, and since the

critical angle squared is proportional to the unit decrement of the index of refraction, δ, and thus is proportional to the density, we conclude that there is no gain of intensity by using more dense mirrors. For mirrors cut at the critical diameters, the intensity is independent of the material of the mirror.

In fact, by using the smaller mirror, say of glass, the sample size is reduced, and also the aberrations are reduced.

10. Optimum Mirror and Camera Dimensions

By combining the aberration equation (38) with that for the solid angle included by the mirror (36) we obtain the relation for the angular width of the circle of confusion

$$\Delta\epsilon = \frac{\rho}{a} = \frac{1}{2\pi}\left(\frac{\Delta\Omega}{\theta_c}\right)\frac{\Delta R}{R}$$

Now since θ_c is proportional to the wavelength, and since the angle of scattering is also proportional to the wavelength, the angular resolution may be written as

$$\frac{\Delta\epsilon}{\epsilon} \propto \Delta\Omega\left(\frac{\Delta R}{R}\right)\left(\frac{1}{\lambda^2}\right) \qquad (40)$$

This expression is not exact, of course; nevertheless it indicates that for a given precision of mirror construction, and for a given solid angle presented to the source by the mirror, the angular resolution improves with the square of the wavelength, and is independent of the size of the camera. The method is thus most

suitable for long wavelengths.

Besides the requirement for a large solid angle and for a high angular resolution, there remains the equally important requirement for a high intensity-to-background ratio. All diffraction methods have a background of stray radiation either due to diffraction or scattering off of slits, from general radiation off of crystals, from the radiation in the "wings" of a crystal rocking-curve, or, in this instance of total-reflection focusing, from diffraction off the edges of the mirror and from irregularities of the mirror surface. In order to reduce such effects, it is necessary to introduce a stop between the mirror and the sample which does not touch the main beam, but which cuts off a large component of the stray radiation. The effectiveness of such a stop is increased by having a large distance between the mirror and the stop position. For this reason, therefore, it was felt advisable to use a relatively long geometry, with at least 50 cm. between the mirror and the film.

In order to accomodate the desired radiations, Cu-L (13.3 A), Ni-L (14.5 A), and O-K (23.6 A), we choose the smallest θ_c (for Cu) which is .0375 radians. So as to include part of the "tail" of the cut-off region thereby allowing the reflection of the small fraction of the line radiation which would be otherwise "cut-off", a value of .034 radians was chosen. By constructing the mirror from a blank of Dow Corning's Precision-Bore Pyrex tubing of 1.500" diameter, the distance between the point source and the point image is of the desired magnitude, 110 cm.

11. Grinding the Mirror - The Problem

The problem was to grind the inside surface of a straight glass cylinder 1.5" diameter, and 4.5" long, into a surface of revolution of an arc radius of approximately thirty-four feet. This radius must be accurate to within a tolerance of two percent. The "barrel" shape is about .0038" deeper in the center than at the edges. A circular arc would deviate from the ideal elliptical arc at the edges by about one ten-thousandths of an inch. Since the spherical aberration introduced by this deviation was shown to be negligible for the geometry used, an attempt to obtain an elliptical arc rather than a circular arc would be unwarranted.

The writer could find no previous literature on methods for constructing such a mirror, and the optical workers of this area differed widely as to suggested methods of approach. Nevertheless, the first method that was tried resulted in a successful mirror.

The approach was twofold: (1) A lap was designed which would permit an optimum use of the natural tendency for a "short" lap to generate an accurate circular arc under a long-time random process. (2) A method was devised for measuring the arc to better than one ten-thousandths of an inch which could be applied to a ground surface as well as a polished one.

12. The Lap Design

A photo of the lap which was used is shown in Fig. 17. It consists of a rectangular piece of cast iron which "rides" in and out of the cylinder along two edges of contact. The lap is pivoted freely

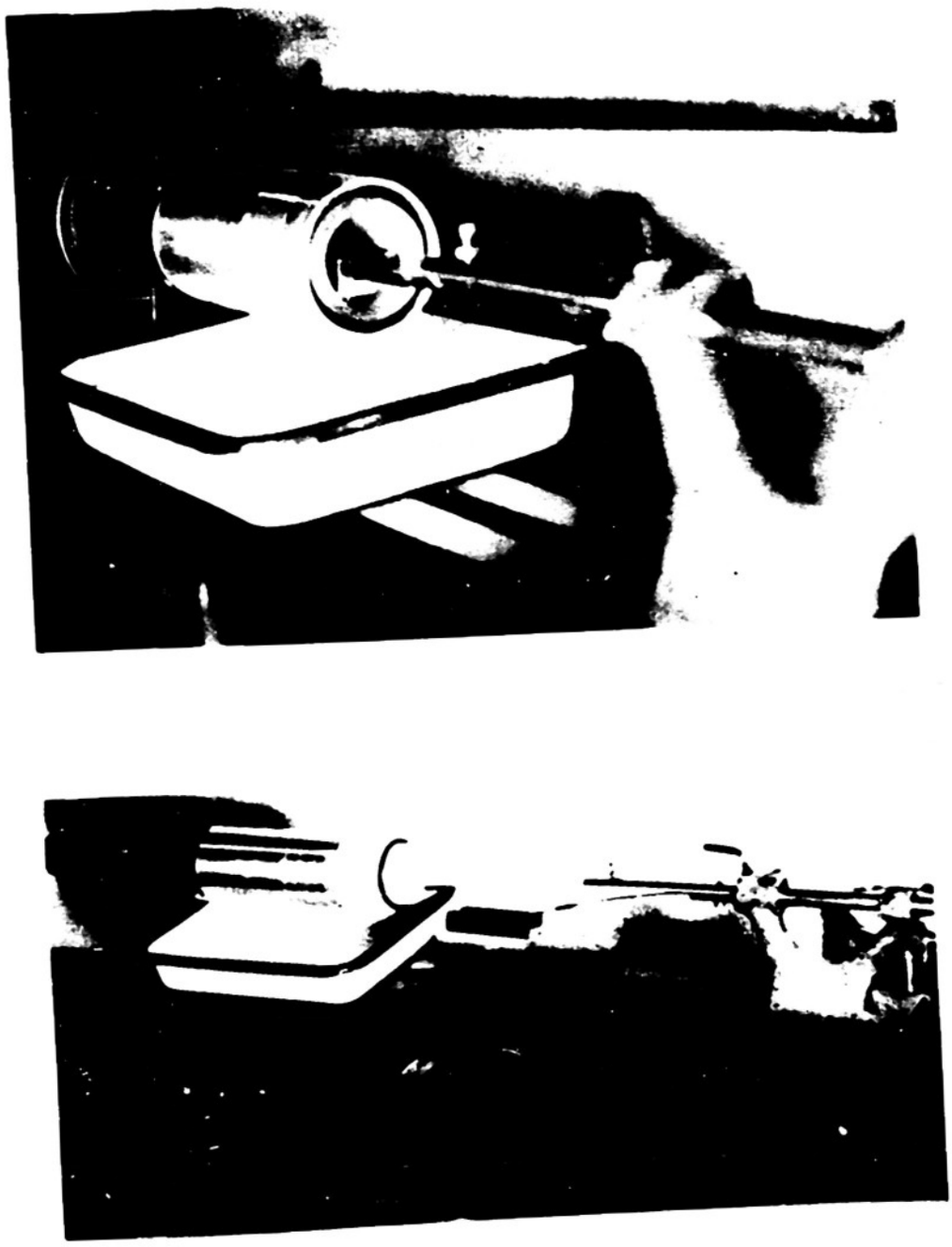

Fig. 17 Lapping Fixture

about an axis as indicated, and is spring-loaded against the mirror surface. The lap is moved back and forth by hand while the mirror is turned by motor one revolution per second. About one and one-half lap strokes for each revolution of the mirror was typical. The spring loading was adjusted so as to provide enough tension to prevent "chatter", and to insure smooth travel.

Since the lap is about one-half the length of the mirror, more grinding action occurs in the center region, and the mirror becomes barrel-shaped. The cast-iron wears away about as rapidly as does the glass in grinding when <u>equal</u> areas are in contact. Consequently, the lap edges conform rapidly to the curvature of the surface because of the relatively small area of contact presented by these edges. For this reason, the lap tends to generate a uniform curvature, i.e., a circular arc, along the lines of contact.

By letting $x = c$, the half-width of the lap, in the equation of the desired surface of revolution

$$\frac{x^2 + y^2}{b^2} + \frac{z^2}{a^2} = 1$$

we obtain an elliptical curve

$$\frac{y^2}{b^2\left(1 - \left(\frac{c}{b}\right)^2\right)} + \frac{z^2}{a^2\left(1 - \left(\frac{c}{b}\right)^2\right)} = 1$$

which is accurately approximated with the geometry used here by a circular arc of radius from (33)

$$R = \frac{a^2}{b}\left(1 - \left(\frac{c}{b}\right)^2\right)^{1/2}$$

So it is evident that the arc generated by the lap along the lines of contact produce another circular arc in the principal plane of radius which is longer by the factor $1/\sqrt{1 - (c/b)^2}$. Also, any irregularities in the lap-arc are demagnified by the same factor.

Another advantage of this lap design is that by virtue of using two lines of contact, it more or less guides itself.

13. Measurement of the Mirror Contour

By carrying out the grinding method outlined above over a relatively long period of time, as required with the fine emery used, one may approach the desired curvature quite slowly. A frequent measurement of the contour during this process would permit precise control over the grinding, allowing adjustment of the stroke used in the lapping if necessary. With the aid of such a measurement, the grinding may be stopped when the exact curvature desired is obtained. Subsequent polishing would not change this curvature to any appreciable extent.

To provide such a measurement of the inside diameter of a ground cylindrical surface to within a precision of better than one ten-thousandths of an inch, an air gauge was designed. An accurately-round ball bearing, a few thousandths of an inch smaller in diameter than the mirror is suspended inside the cylinder. A constant flow of air is passed through, and the pressure drop across the ball is measured with a manometer. As the ball is lowered into the cylinder the pressure difference becomes less as the contour of the mirror deepens, since more area and less resistance is presented to the air stream flowing

through the clearance between the tube and the sphere.

A schematic and a photograph of the air gauge are shown in Fig. 18. At the compressed air outlet a pressure regulator is inserted into the line, followed by a long capillary to the gauge itself. This arrangement presents a steady, "constant-current" source of air. The air line is connected to the mirror cylinder through another cylinder-ball path of practically the same dimensions. The small pressure drop developed across each annular orifice is measured by an inclined water manometer. The orifice of the first cylinder-ball path is held constant, while that in the second will vary as the ball is lowered into the ground cylinder. The respective pressures measured are P_o and P.

The values for the air-flow velocities used in this arrangement yield Reynolds numbers which indicate that the mass of air that passes through the system per unit time would not depend very much upon the effects of viscous forces, and certainly not upon the effects of the compressibility of the gas since the velocities involved are negligibly small compared with the pressure wave velocities. Dimensional analysis allows us to write immediately a relation for the mass flow per unit time, Q, which passes through the first cylinder

$$(A) \qquad Q = A_o \sqrt{\rho P_o}\, f_o\left(\frac{Q}{\mu t_o}\ ,\ \frac{t_o^2}{A_o}\right) \qquad (41)$$

in which A_o is the orifice area, ρ is the density of the air, μ is the dynamic viscosity coefficient, t_o is some significant linear dimension, which in this problem, would be the difference in radii

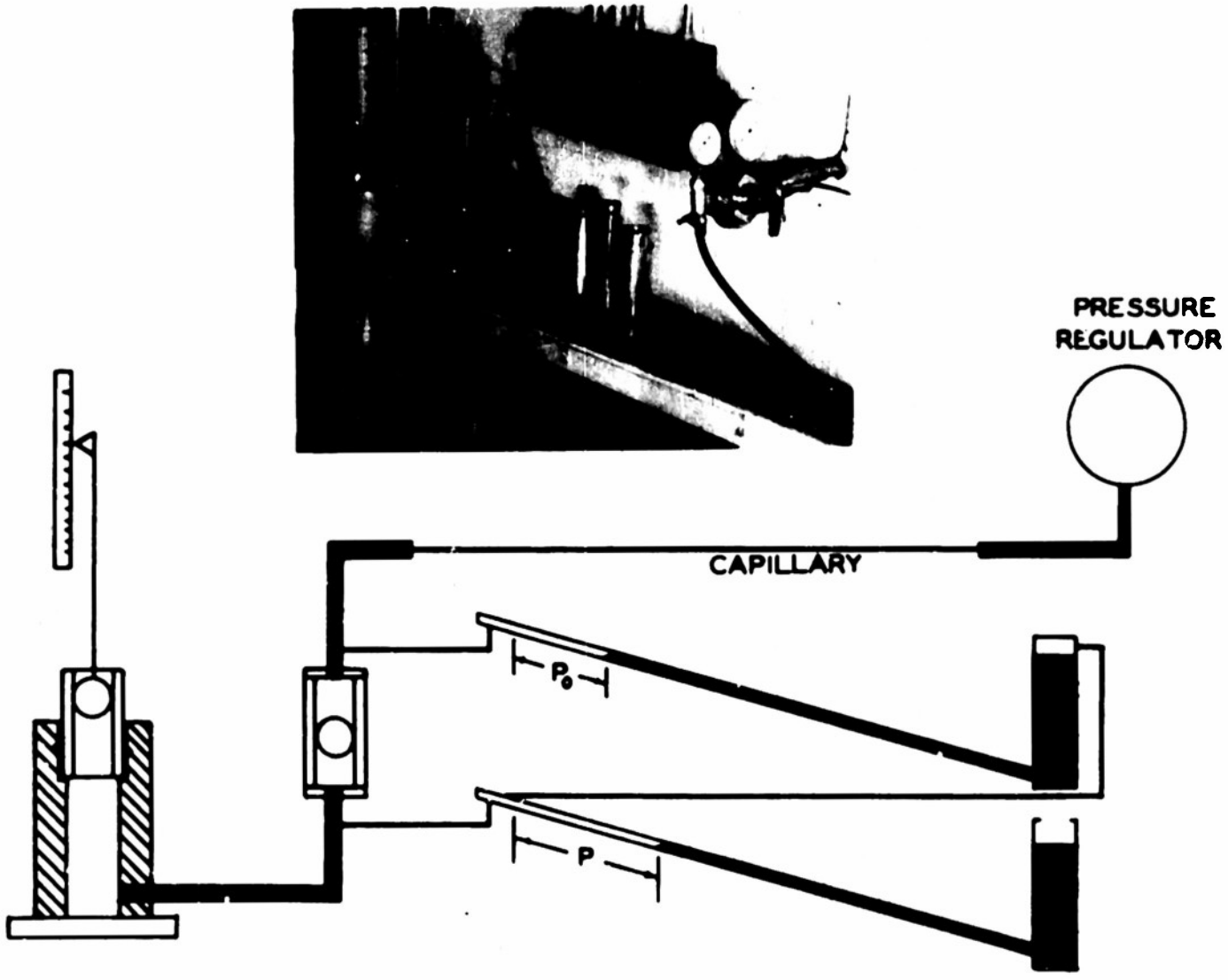

Fig. 18 AIR GAUGE

of the ball and the cylinder, and f_o is chosen to be the viscosity - dependent factor. Since we would not expect a very appreciable effect due to viscous forces, it follows that the function f_o would be a very slowly varying function for the range of Q used. Now we may write a nearly identical equation for the Q that passes through the second ground cylinder. Equating these relations, because the same Q passes through both cylinders, we obtain

$$(B) \qquad A_o \sqrt{\rho P_o}\, f_o \left(\frac{Q}{\mu t_o}, \frac{t_o^2}{A_o} \right) = A \sqrt{\rho P}\, f \left(\frac{Q}{\mu t}, \frac{t^2}{A} \right)$$

and since the orifice area is almost exactly equal to the circumference of the ball times the clearance t, we may write

$$(C) \qquad t = t_o \left(\frac{D_o}{D} \right) \sqrt{\frac{P_o}{P}} \; \frac{f \left(\frac{Q}{\mu t_o}, \frac{t_o^2}{A} \right)}{f \left(\frac{Q}{\mu t}, \frac{t^2}{A} \right)} \qquad (42)$$

D_o and D are ball diameters. The functions f_o and f are identical because of the similarity of the two orifices. Since the arguments of these functions are of the same order of magnitude and since they are slowly varying functions as discussed above, their ratio should approach unity. Consequently,

$$t = t_o \left(\frac{D_o}{D} \right) \sqrt{\frac{P_o}{P}} \qquad (43)$$

which permits the measurement of the contour of the mirror.

By means of this method, based on relative pressures measured across exactly similar orifices, one notes that the dependence on air density drops out. Also, since the thermal expansion coefficients of the glass and the steel bearings are nearly the same, there is no

measurable change in t due to differential expansions caused by ordinary temperature variations. So it is seen that the method is very insensitive to temperature variations, a factor which is, of course, all-important in precision measurements of extremely small distances.

Moving the bearing about at any particular position within the mirror cylinder does not appreciably change the pressure reading, but in order to present a constant geometry of orifice to the air flow, the bearings in both cylinders were placed in contact with the side of the cylinder.

In order to verify the derived relationship (43), and to calibrate the gauge, the following method was used. All measurements of a particular contour were made with two ball-bearings of approximately .003" difference in diameter. The measured values of the inverse square root of the pressure drop, p, were plotted against the axial position of the ball along the mirror for each of the ball-bearings. The relationship for t, (43), is verified by the fact that these curves are always identical and are displaced by a constant amount, which corresponds to the difference in their radii. In this manner also, a calibration of the contour curves is obtained, based on a known difference in the ball radii.

It was desired, therefore, to know this difference in radii to within .00001" if possible. We are very much indebted to D.O. Hendrix* who made this measurement with the arrangement shown in Fig.19. Two stacks of steel gauge blocks were used, one slightly higher and the other slightly lower than

---

* Mt. Wilson and Palomar Observatory.

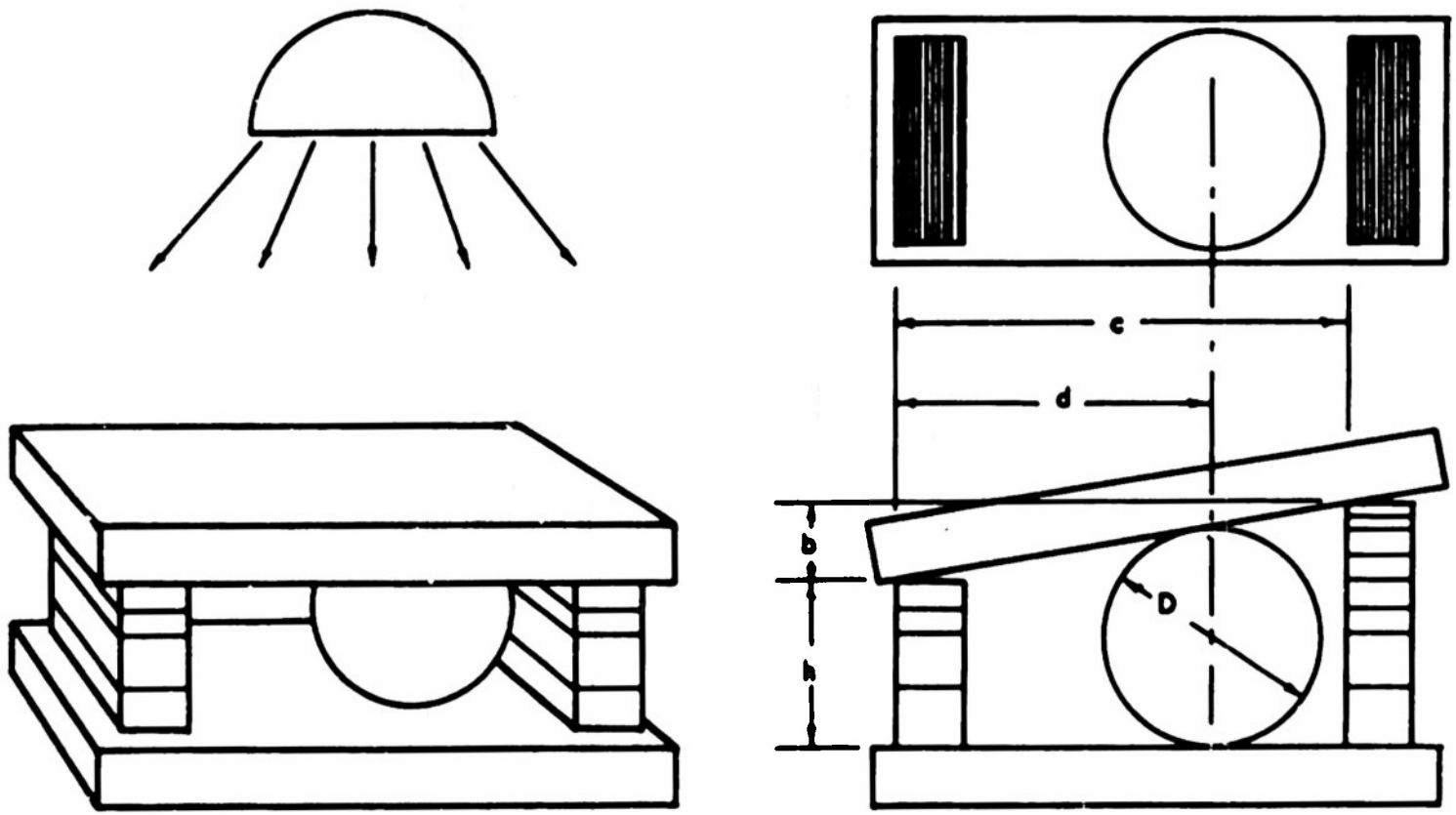

$$D = h + b\left(\frac{d}{c}\right)$$

Fig. 19 MEASUREMENT OF SPHERE DIAMETER

the diameter of the bearing to be measured. These stacks were placed upon an optical flat, and another optical flat was placed across the top of the gage blocks. Interference fringes were observed under this flat, between it and the top of the gauge blocks. Now the ball was moved from the taller stack toward the shorter until contact was made. Contact was indicated by a resulting shift in the interference fringes. Knowing the distances, a and b, and the difference in the gauge block heights, it is a simple calculation to determine the bearing diameter.

These bearings were chosen at random from a stock of ordinary commercial ball-bearings. They were spherical to within .00001". The diameters of the two bearings used in this work were measured in this way to be 1.49994" and 1.50268", with a difference in their radii of .00147". This last number, then, is the distance corresponding to the displacement of the curves taken of the same contour with these two bearings.

Approximately one hour was required to measure a given mirror contour in this way. These measurements were found very convenient in the initial stages of the grinding in that they showed the rate of change of the contour with time of grinding, and permitted one to adjust the type of lap stroke to use in order to obtain the desired shape of the contour. The first and the last measurement which were made on the mirror are shown in Figs. 20 and 21. It was found that the contour measured for a finely ground surface and that for the subsequently polished surface were identical. The fact that this gauge works equally well for ground surfaces is of course a great advantage over optical testing methods.

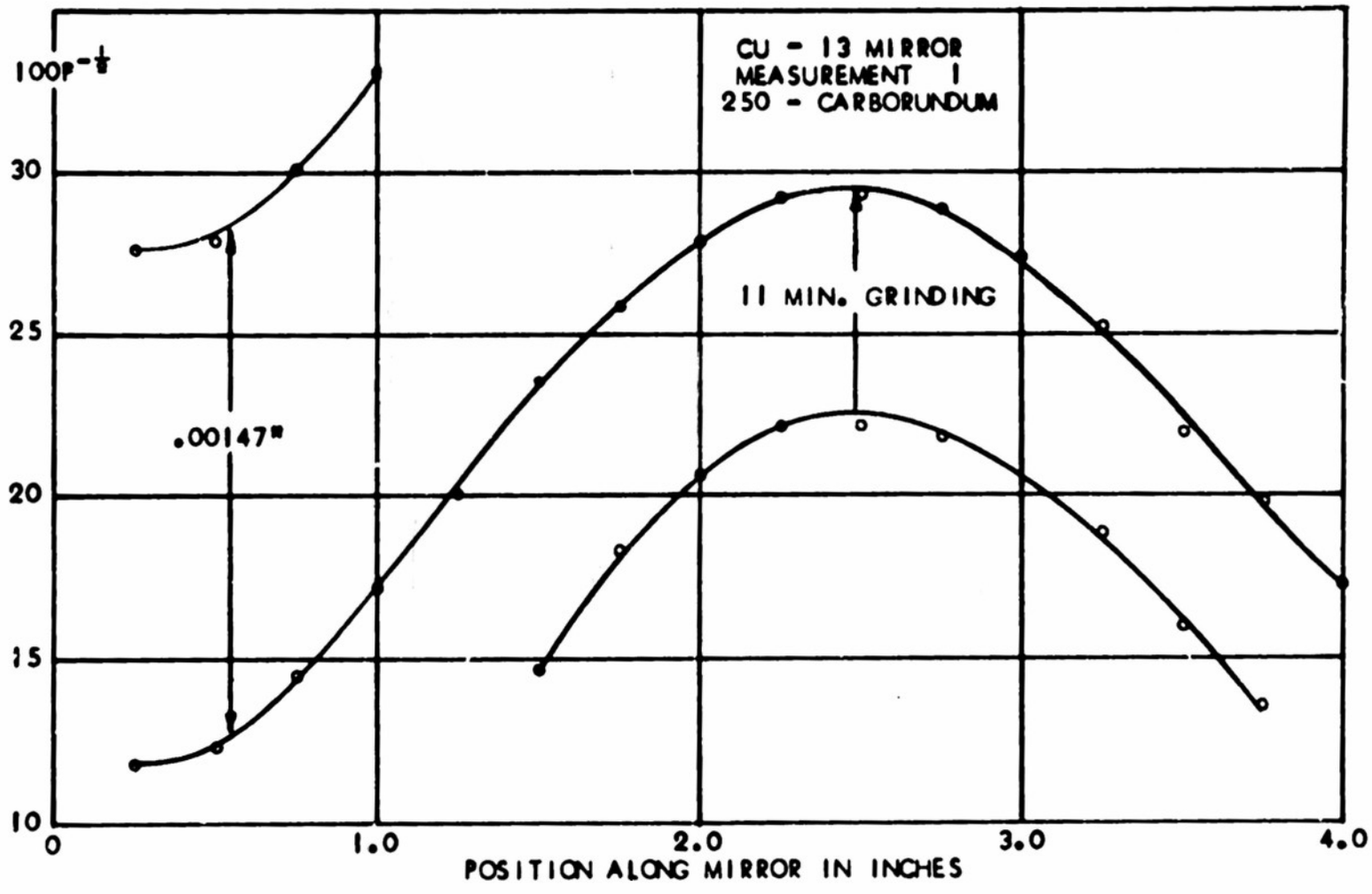

Fig. 20 AIR GUAGE MEASUREMENT OF RATE OF GRINDING

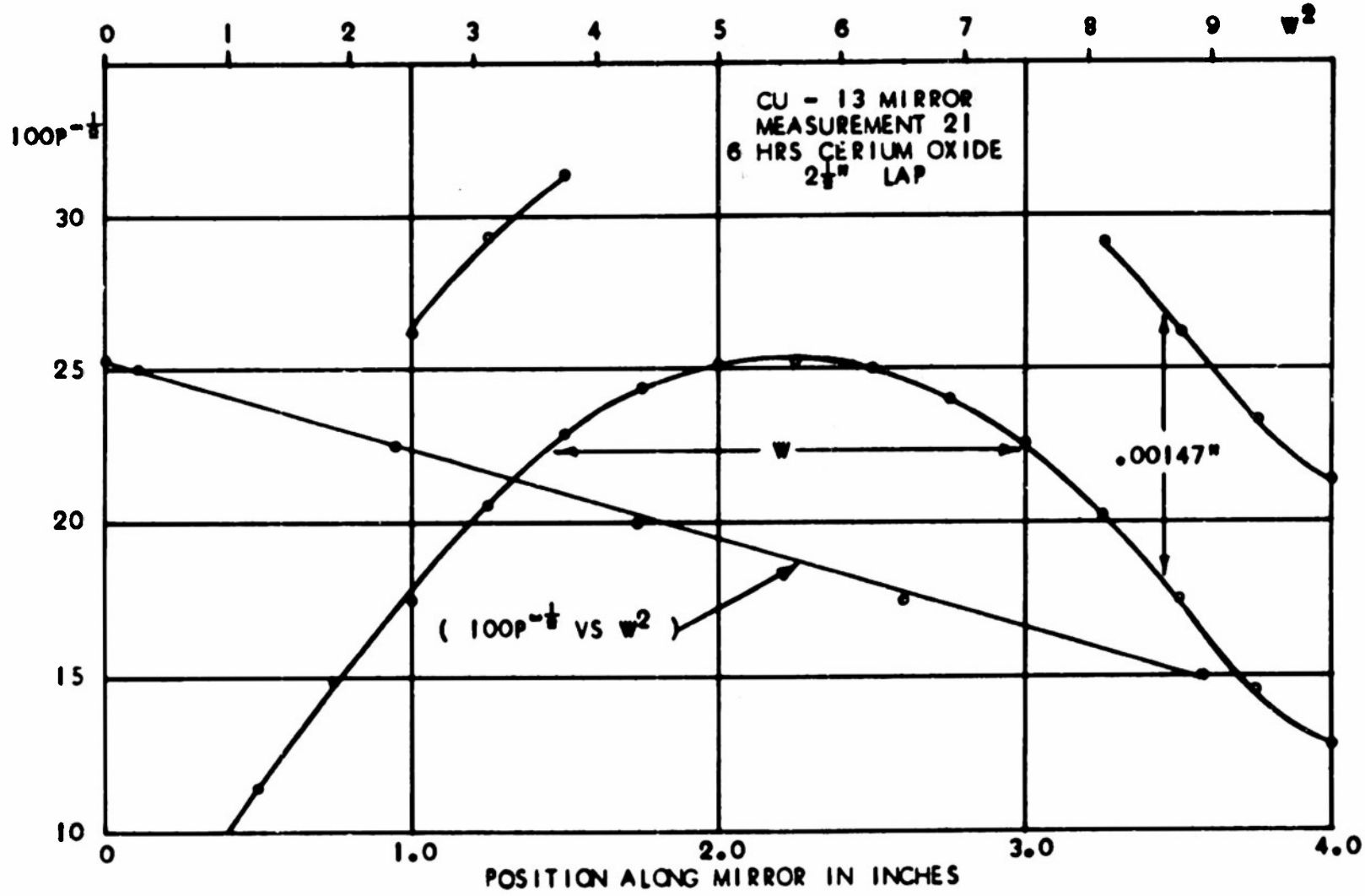

Fig. 21 AIR GUAGE MEASUREMENT OF MIRROR FIGURE

14. The Polishing of the Mirror

The polishing lap was constructed from the same lap used in grinding by facing its already contoured edges with strips of red dental wax. Somewhat less spring tension was used between the wax lap and the mirror. Cerium oxide and red rouge were used in a water suspension as the polishing agent and lubricant. The lap was moved back and forth by an eccentric on an electric motor, so that there were about three strokes of the lap for each revolution of the mirror. The eccentric motor was non-synchronous and so its speed was not constant, therefore there was no possibility for any periodic effect being introduced.

After fifty hours of polishing, there was no appreciable change of the radius of curvature, and the surface appeared smooth under microscopic examination. As discussed below, another fifty-five hours of polishing were applied to the mirror in order to determine if any appreciable difference could be found in the character of its x-ray point-image. There was no measurable change, thus it was felt that further polishing would not be necessary.

15. Testing the Mirror

After the first fifty hours of polishing the surface appeared free of pits under the microscope. It was then set up on the optical bench with a suitable source-image point geometry as indicated by the air-gauge measurements. A Cenco point source was used. A very sharp image of the source was immediately obtained, and the position as predicted by the air-gauge measurements seemed to be optimum. The

depth of focus for such a small aperture system is so great, that this optical method for testing the geometry of the mirror is relatively insensitive.

The mirror was then mounted in the x-ray diffraction camera. The type of mounting used, and the mechanism for its adjustment are shown in Fig. 22.

Photographs of the point image of a .010" pinhole source were taken for several different exposure times. For the short exposure image, very little broadening is indicated. However, prolonged exposures showed considerable broadening. This broadening is greater than that which could be accounted for by halation effects.

It was soon discovered that this stray radiation was not caused by a diffuse scattering; the radiation does not leave a point of the mirror and spread out in a uniform distribution of angles within a cone of radiation as might be expected, for example, from irregularities in the surface of the mirror. Instead, this stray radiation casts a sharp shadow of the spiders which support the central stop behind the mirror position indicating that the unfocused ray leaves the mirror and remains in a plane that includes the central axis of the optical system. Photographs which illustrate this transverse scattering effect are shown in Fig. 23.

The first step which was taken in the attempt to discover the cause for the stray radiation was to polish the mirror for another fifty-five hours. However, after identical tests were made as described above, there was found no decrease in the amount of stray radiation.

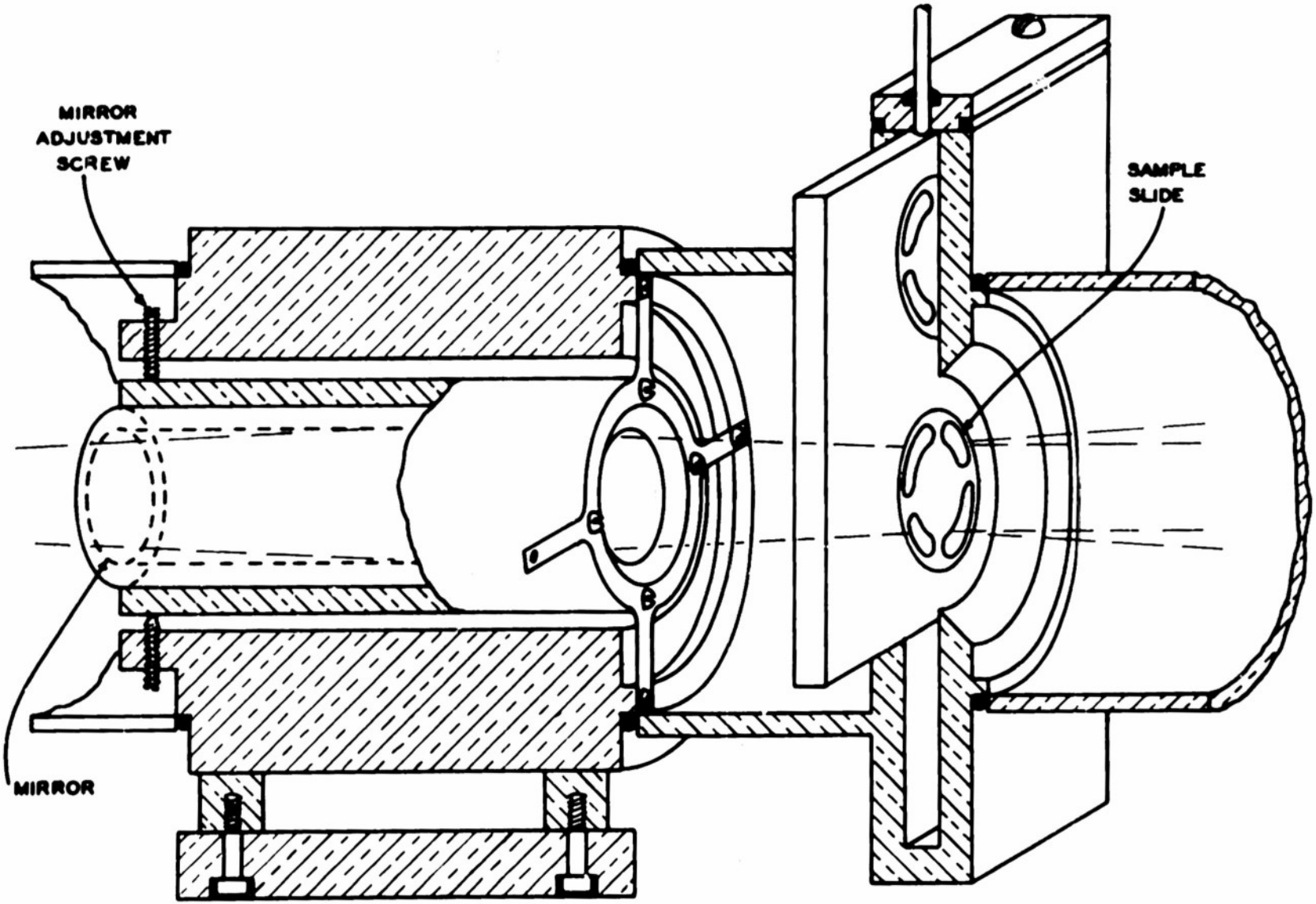

Fig. 22 MIRROR MOUNT
AND SAMPLE SLIDE

Next, the mirror was placed back on the optical bench and a photograph was taken of the mirror itself with the camera placed along the axis of the mirror at a position beyond the focal spot. In the first picture that was taken, only light which passed through a .5 mm. pinhole placed at the focal spot was used to make the photograph. This picture showed an even illumination of the mirror surface, demonstrating that all parts of the surface were contributing to the focal spot, and that the curvature of the mirror was uniform and correct. Then a photograph was taken of the mirror from the same position with the pinhole still in the image plane, but displaced 2 mm. below the focal spot so that only stray radiation reaching this point would form the photographic image. This time only the very top and bottom portions of the front and back edges of the mirror were "lighted up". It seemed certain that this stray light radiation was due to Fresnel diffraction from the edges of the mirror.

In order to prove that Fresnel diffraction from the edges of the mirror accounts for the stray x-radiation, a pinhole photograph might be taken of the mirror with the pinhole placed again at the image plane and just out of the region of the focal spot. However, because this stray radiation is so weak relative to the main focal spot intensity, no such photographs have been obtained as yet, even with a 200 hour exposure

Ehrenberg[54] has observed a similar effect in the broadening under prolonged exposure times of a line image formed by a curved glass reflector. He has found evidence also for the diffraction off the edges of the mirror. However, he believes that another contributing

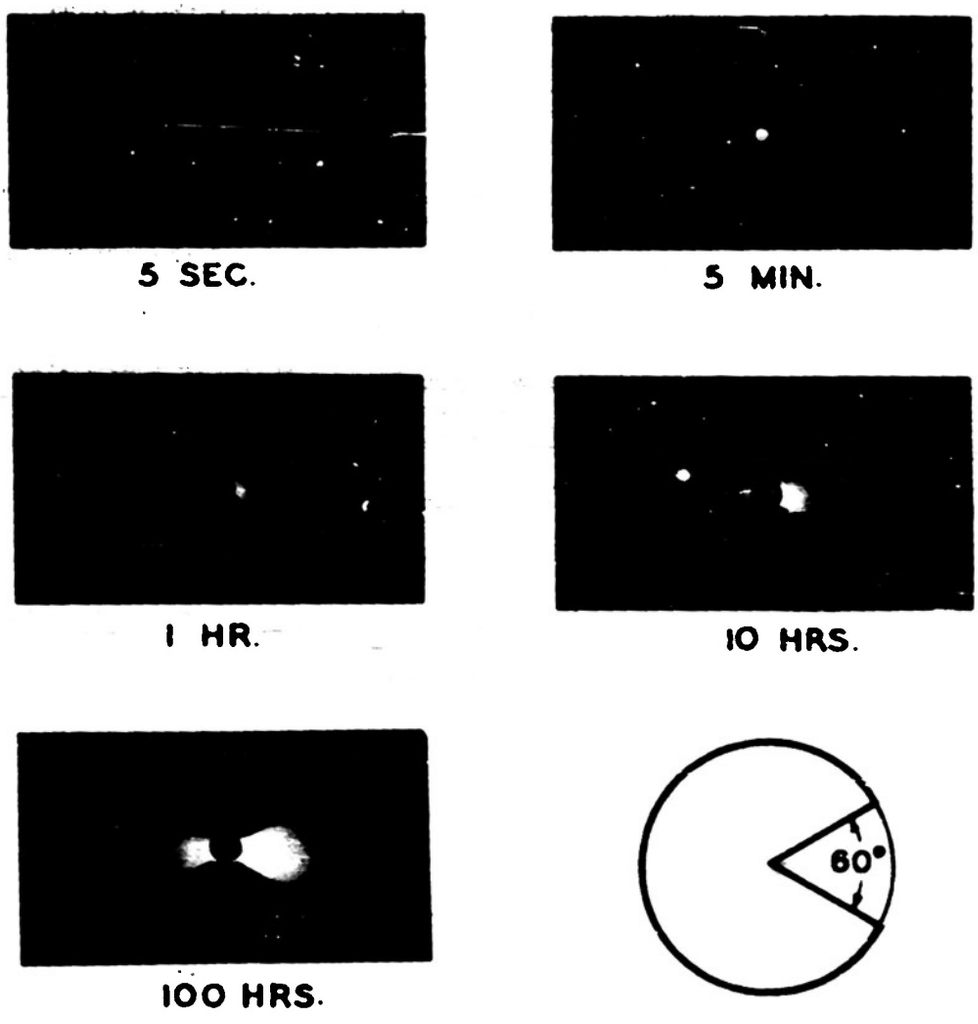

Fig. 23 Actual size of center-hole in film is .040 inch

cause for the broadening is due to a diffraction from "ripples" in the surface of the polished glass. He calculates that these have heights above the average surface level of about 10 A.U. He gives no explanation for the existence of such surface structure.

The writer hopes to do a great deal more work on this problem because it seems to hold the answer to the question of the practical resolution limit of the total-reflection method which is of interest in this application, and of course, also in the field of x-ray microscopy. As was discussed above, all types of low-angle diffraction units exhibit this kind of background radiation to a greater or lesser extent. Whether or not the concave mica method, for example, will allow higher resolution depends upon whether its focal spot broadening effect is as great as that of the total-reflection method. In any event, the use of long camera geometry, and of stops placed just in front of the sample, will minimize the effect of the background, limiting this to the region near the focal spot. For long wavelengths, the data of interest is rarely obtained from this region.

16. Long Wavelength Photography

Because the intensity of a low-angle diffraction pattern is characteristically low, photographic detection seems to be most appropriate. Counter techniques demand high stability of the x-ray source, and often, for the long periods required to obtain good statistics in counting, such stability cannot be obtained. This is particularly true for the gas-type tube.

Another advantage of the photographic method may well lie in

the possible use of an especially designed microphotometer, which, in effect, utilizes a circular window slit of variable diameter. In this way, all of the radially symmetric pattern contributes to the measured data. The effect of film grain would thus be minimized, and lower densities could be used. Such a microphotometer has not been constructed as yet. However, a possible design is indicated in Fig. 24.

A very thin cone-shaped beam is formed by the reflection from a narrow ring shaped mirror, of the light from a point source, as shown. In this way, the light is focused into a small pinhole window of a photo-tube. The low-angle diffraction photograph is centered on the axis of the ring mirror and mounted perpendicular to it. As it is translated toward the photo-tube, the thin circle of light through the film changes in radius, but its total flux is constant. The photo-tube reading measures the transmission of the film for a given radius from the center of the pattern. This transmission is decreased by both the absorption and the scattering due to the exposed grains, thus affording a maximum sensitivity to exposure. Since all light rays strike the film always at the same angle throughout a complete measurement of the film, the loss due to reflection off the film is a constant, and therefore does not affect the measurement. The carriage which translates the film may also hold the paper on which the recording galvanometer pen writes. In this way there is a direct linkage without the possibilities of such error as introduced by screw systems.

For ordinary x-rays, the measurement of relative intensities is made easy because of the strict proportionality between the intensity and the film density ($\log_{10}$ 1/transmission). This relationship holds

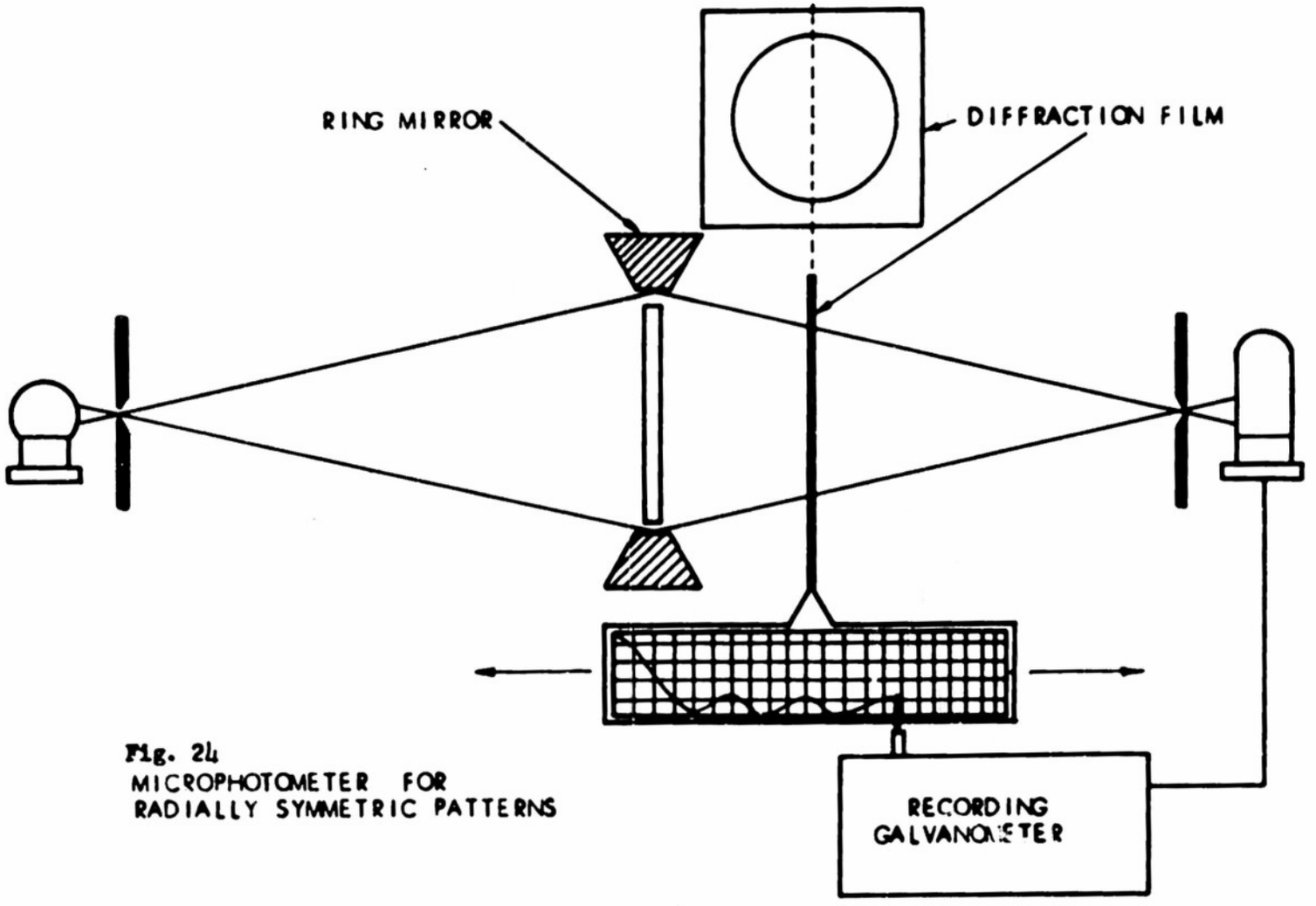

Fig. 24
MICROPHOTOMETER FOR
RADIALLY SYMMETRIC PATTERNS

up to densities as high as .6. However, it has been found that for Cu L (13.3 A) for example, the intensity versus density curve is linear only up through a density value of .3. For higher densities the logarithm of the intensity is proportional to the density. This result was obtained from Eastman Medical X-ray film, but it probably holds also for approximately the same density regions for other films of this type.

The sensitivity of photographic films for the long wavelengths is also considerably less than that for ordinary x-rays, such as Cu (1.54 A). This is due to the absorption in the surface layers of the gelatine which prevents a large component of the beam from reaching the sensitized emulsion.

Relative sensitivities of several types of film were determined by exposing simultaneously small sections of each to a broad beam of copper-foil-filtered Cu-L (13.3 A) radiation. These were developed for five minutes in Eastman's D-19 developer of normal strength. Listing the film in order of their densities for the same exposure time, giving that of highest density first:

Ilford, Industrial Type G

Kodak Medical X-ray

DuPont, Hi Speed Pan (with no over-coating)

Kodak, Short Wave Response

A sketch of the film mount is shown in Fig. 25. The circular film and an accurately centered hole, .040 inches in diameter, are cut in a single operation with an especially constructed film punch.

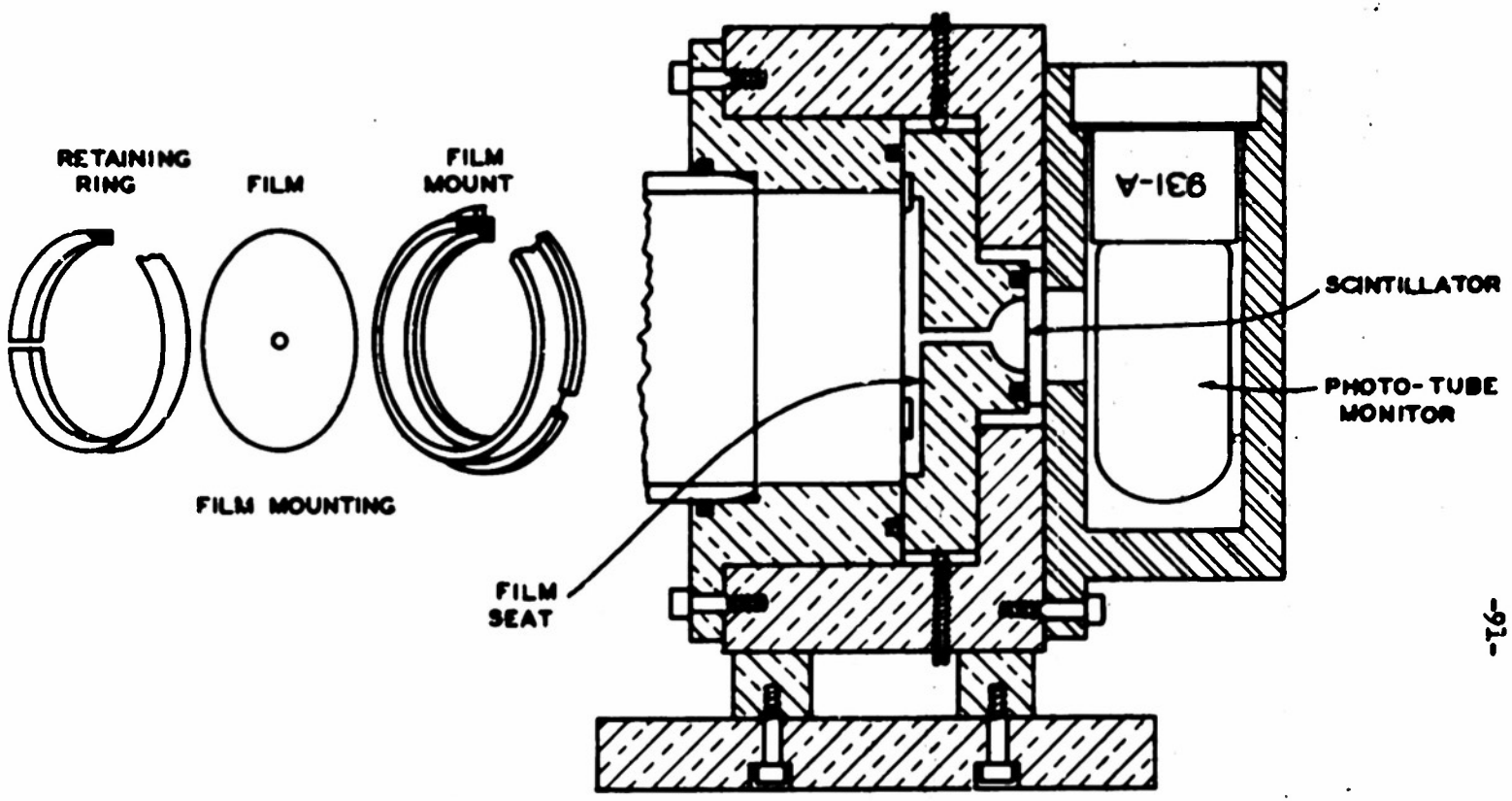

Fig. 25 FILM MOUNT AND PHOTO-TUBE MONITOR

The film holder locks into a section, as is indicated, which can be moved perpendicular to the axis of the camera by means of set-screws from outside the vacuum. With this adjustment it is then possible to pass the direct beam through the center of the film hole.

17. The Photo-Tube Monitor

The direct beam, after passing through the central hole in the film, then strikes some fluorescent material located in a thin film in the center of a glass window as shown in Fig. 25. A large solid angle of the light radiation from this material is utilized by placing a concave mirror immediately behind the window. This means of measuring the intensity of the direct beam permits (1) an adjustment of the focal spot on the anode for optimum intensity; (2) the absorption within the sample and the proper sample thickness can be determined from the direct beam intensities with and without the sample in place; (3) an accurate determination of exposure can be made directly, rather than determined indirectly from the tube voltage and the tube current.

18. The Associated Equipment

A photograph of the associated equipment along with the total reflection diffraction unit is shown in Fig. 26. In the foreground are the regulated power supply for the 931-A photo-tube monitor, a vacuum tube voltmeter for reading photo-tube output, a kilovolt meter, and a milliameter for the x-ray tube power supply.

This high voltage supply is a voltage doubler designed to operate at voltages up to 15,000 volts at about 400 watts. A Variac

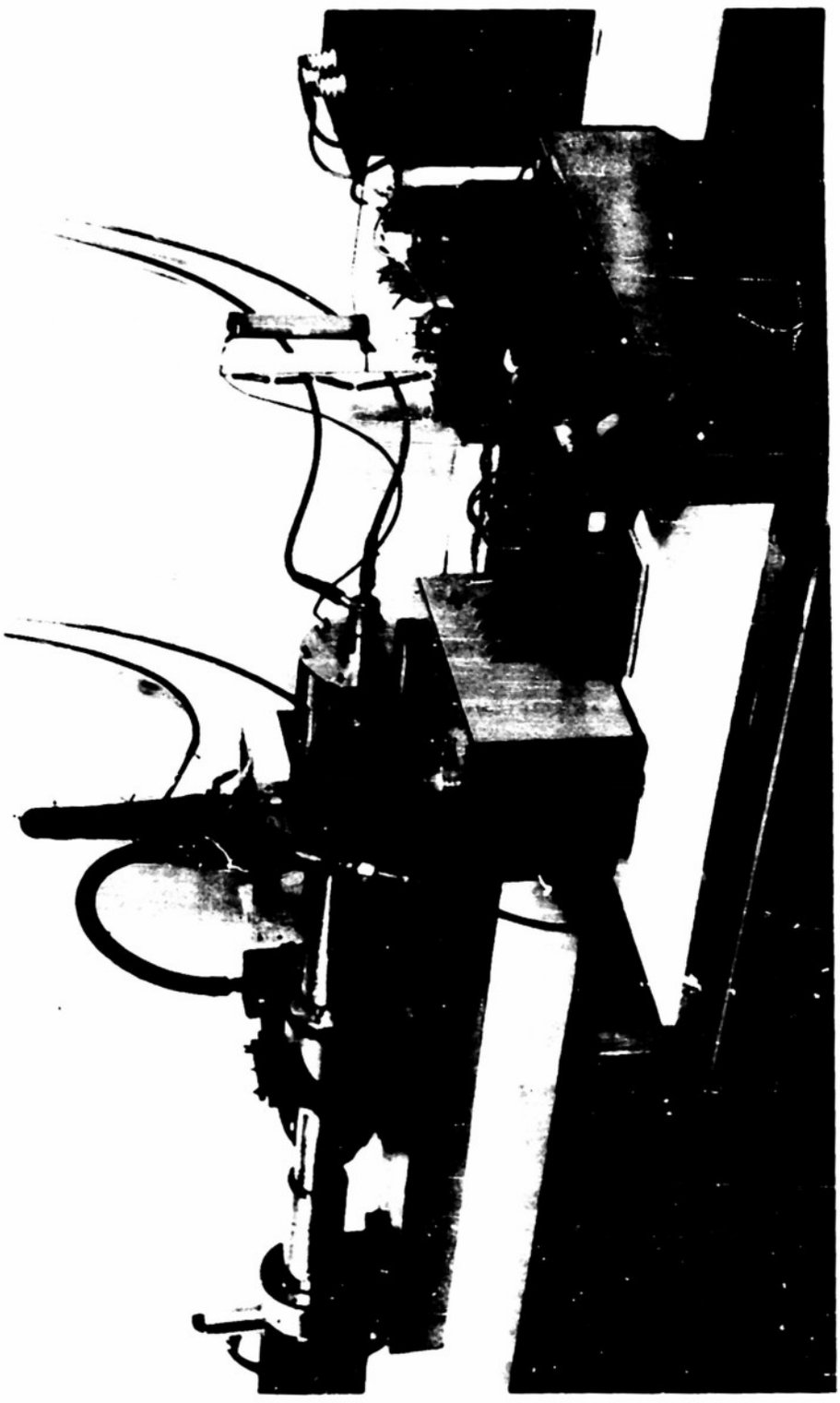

Fig. 26 Photograph of associated equipment

is used on the input of the high voltage transformer to vary the tube voltage. A 10,000 ohm resistance is inserted in series with the anode to provide the desired regulation.

The vacuum system consists of a D.P.I. oil diffusion pump backed by a Welch mechanical pump. In order to permit the rough-pumping out of the camera through the diffusion pump, silicone oil is used thereby eliminating the need for an elaborate valving system. With this arrangement a sample reloading cycle of about twenty minutes is possible.

About fifteen feet of one-quarter inch rubber hose has been found sufficient insulation in the cooling water lines between the anode and ground potential. The x-ray tube cooling system and that of the diffusion pump are in series.

V. THE APPLICATION OF THE TOTAL REFLECTION DIFFRACTION UNIT

1. A Measurement of the Monochromaticity of the Focused Radiation

As described above, the first mirror which was constructed produced a relatively intense focal spot. With the use of stops, the stray scattering was minimized and a suitable angular resolution was obtained. The degree of monochromatization remained to be evaluated before the instrument was to be used for low-angle diffraction measurements.

In order to measure the monochromaticity of the focused radiation, a small spectrograph was designed to fit into the film holder position. With this instrument a focused spectrogram is produced measuring wavelengths up to about 20 A.U.

A sketch of the spectrograph is shown in Fig. 27. The converging x-ray beam from the mirror strikes a small cylinder of mica crystal so that all angles from 0° to 90° incidence are presented. Since the spacing of the cleavage planes of mica is 9.9 A.U., this permits Bragg reflections up to 19.8 A.U. Nearly all such reflections are focused onto a circular arc which passes through the image point and along which a film is placed. The resulting positions of a few of the wavelengths of interest here are indicated.

A spectrogram was taken with unfiltered Cu-L (13.3 A) radiation with the x-ray tube at 4000 volts. A well focused spot image was formed at the expected position on the film for the 13.3 A.U. radiation and with no effective background radiation at any other wavelength.

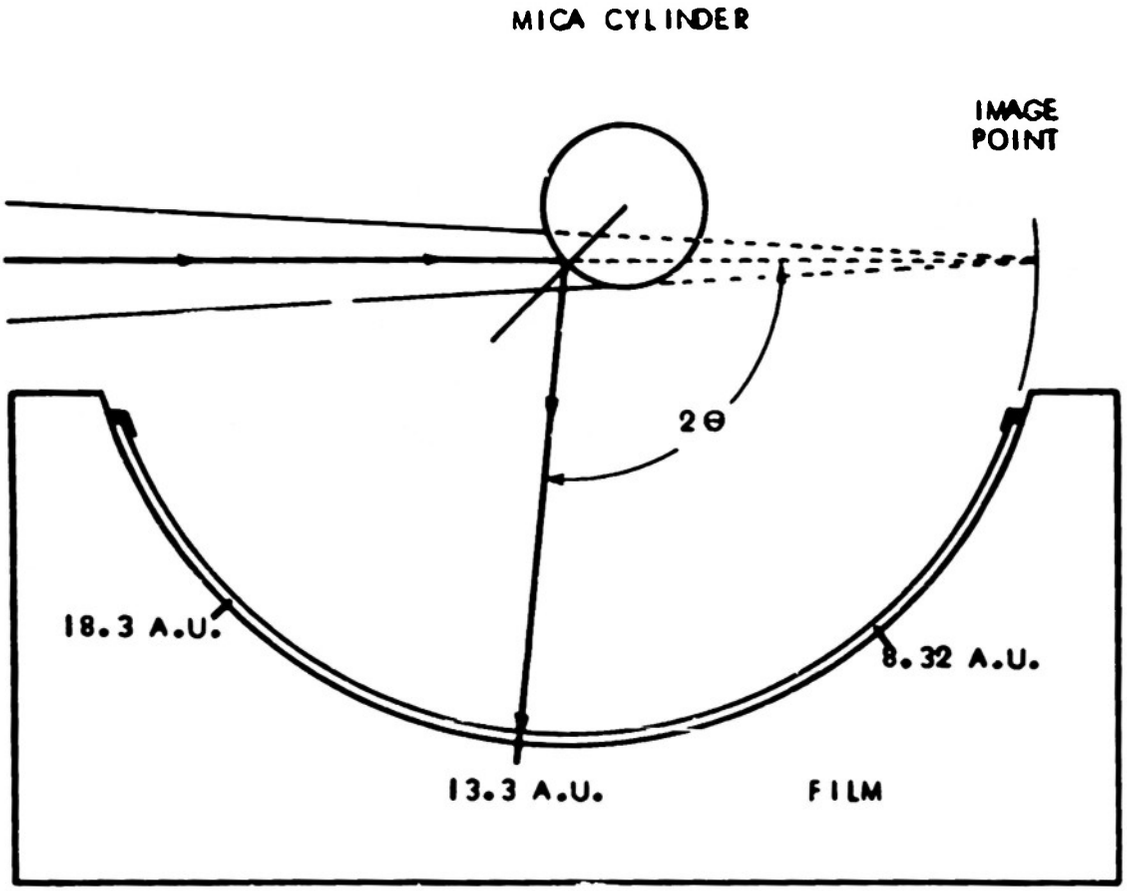

Fig. 27
AN INSTRUMENT FOR CHECKING THE MONOCHROMATICITY OF THE POINT-FOCUSED RADIATION

2. A Preliminary Measurement of the Dow Latex Particles

A sample of the same latex material which was studied by Danielson, Shenfil and DuMond[19] was suspended in water solution and re-dried onto a collodion film. A nearly transparent layer of material was formed in this way.

A ten hour exposure of this sample in the total reflection camera resulted in the diffraction photograph shown in Fig. 28. This was taken with the tube at 4000 volts and 20 ma. The Kodak Medical X-Ray film was used which was developed in D-19 for five minutes. The Cu-L (13.3 A) radiation was filtered through two thicknesses of aluminum leaf which was .2 mg per square centimeter mass thickness. The actual distance between the scratches was 1.888 cm. The sample-to-film distance was 19.99 cm.

Recalling that the diffraction parameter, u, is given by the equation

$$u = \frac{2\pi R \epsilon}{\lambda}$$

we may write an expression for the diameter of the particle, D, in terms of the value of u and of the diameter, d, of the ring for a given maximum of the diffraction curve. Thus

$$D = \frac{L\lambda}{\pi}\left(\frac{u}{d}\right) = 84.67\left(\frac{u}{d}\right) \text{ A.U.} \qquad (44)$$

Six microphotometer curves were measured for the six sharpest rings, numbers 5 through 10. Using the values of u for the maxima as

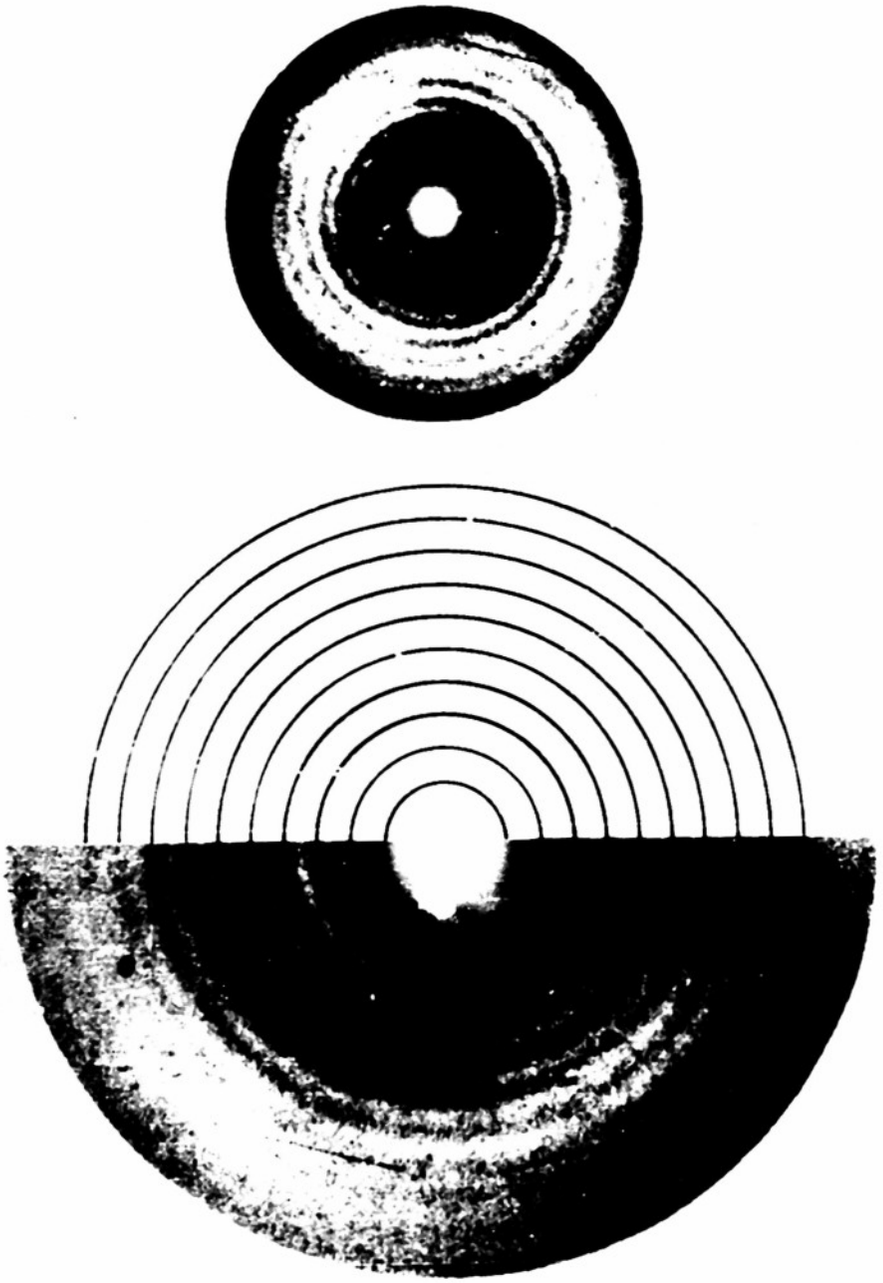

Fig. 28 LOW-ANGLE DIFFRACTION PATTERN OF DOW LATEX PARTICLES (R=1380 A.U.) USING 13.3 AU X-RADIATION.

given in Fig. 2 for a random distribution of spheres, the average value of (u/d) was calculated for each ring. These are listed in the table below.

Ring	(u/d)
5	32.8
6	32.8
7	32.6
8	32.6
9	32.6
10	32.6

In Fig. 28, circles corresponding to a value of u/d = 32.6 are drawn against the diffraction pattern in order to illustrate the extent of agreement with theory. This value of (u/d) may be used in (44) to yield a value for D = 2760 A.U.

The apparent shift in the peaks near the center of the pattern may be explained on the basis of inter-particle interference[57]. Since the material had been re-dried several times before this sample was prepared the material was very likely to have been in clumps of many particles each. Robley Williams* has described in a private communication that the latex is attacked by bacteria and does change in structure unless it is kept in a sterile condition. The sample used here was not kept in this way. Also it has been observed that material dried in the manner described does become coated with a substance which is otherwise dissolved in the water solution. This coating appreciably increases the particle size. For these reasons not very much significance should be attached to the value of the measured diameter as regards to an absolute calibration of the "sterile" Dow latex particles. The purpose accomplished here is rather to

---

* University of California, Berkeley, California

illustrate the possibilities of the new instrument and method.

The relatively short exposure time required for this diffraction photograph, (in spite of the fact that the mirror was cut to less than one-third of a practical working length) and the angular and wavelength resolution which is indicated by the sharpness of the pattern do demonstrate the "hoped-for" performance of the instrument and method.

A sterile sample of the latex particles has been kindly given to us by Dr. Williams. Work is now in progress in the setting up of a technique for the dispersing of these particles into a monomolecular layer of random distribution. These are to be mounted on very thin collodion films in order that the identical sample may subsequently be transferred to the electron microscope for a verification of the randomness and single-layeredness of the dispersion, and to provide a direct calibration of the microscope as well.

3. Extension of the Research and Development of this Long Wavelength Low-Angle Diffraction Method

A program for constructing optimum size mirrors for several different wavelengths is planned. It is of particular interest to develop a mirror which will monochromatize Al-K radiation as discussed above.

It is intended to investigate extensively the problem of focal-spot broadening of a totally-reflected beam in order to learn where the practical limit of application of this method lies.

It is hoped that a microphotometer can be developed, capable of exploring the entire circumference of each ring so as to utilize all

of the radially symmetric pattern and thus better average out the effect of film grain. This would be of exceedingly great value in increasing the sensitivity and precision of the low-angle diffraction method.

Finally, it is planned to begin a program of measurement of particle sizes and shapes in the 100 A.U. to 500 A.U. range of large molecules, virus, and bacteriophage, this work to be done along with parallel studies with the electron microscope.

REFERENCES

1. A. Guinier, Ann. phys. 12, 161 (1939)
2. Lord Raleigh, Proc. Roy. Soc. 84, 25 (1911); 90, 219 (1914)
3. R. Gans, Ann. Physik 76, 29 (1925)
4. G. Mie, Ann. Physik 25, 37 (1908)
5. W. R. Smythe, Static and Dynamic Electricity (McGraw-Hill Book Company, Inc., New York, 1950) second edition, p. 491-3
6. J. A. Stratton, Electromagnetic Theory (McGraw-Hill Book Company, Inc., New York, 1941) Chap. IX, Sections 9.25, 9.26, 9.27
7. V. K. La Mer and D. Sinclair, O.S.R.D. Report, 1857 (September 29, 1943)
8. Tables of Scattering Functions for Spherical Particles, Bureau of Standards Applied Mathematics, Series 4, Washington, D.C.
9. P. Debye, Ann. phys. 30, 57 (1909)
10. H. C. van de Hulst, Optics of Spherical Particles (N.V. Drukkerij, J.F. Duwaer en Zonen, Amsterdam, 1946)
11. R. W. Hart and E. W. Montroll, J. Appl. Phys. 22, 376 (1951)
12. A. H. Compton and S. K. Allison, X-Rays in Theory and Experiment (D. Van Nostrand Company, Inc., New York, 1946) p. 563, 805
13. Jönsson, Dissert., Upsala (1928)
14. E. Dreshem and M. Shein, Phys. Rev. 37, 1238 (1931)
15. B. Woernle, Ann. Physik 5, 475 (1930)
16. G. B. Bandopadhyaya and A.T. Maitra, Proc. Roy. Soc. 21, 869 (1936)
17. J. A. Victoreen, J. Appl. Phys. 14, 95 (1943); 19, 855 (1948); 20, 1141 (1949)
18. R. von Nardroff, Phys. Rev. 28, 240 (1926)
19. W. E. Danielson, L. Shenfil, and J.W.M. DuMond, J. Appl. Phys. 23, 860 (1952)

20. R. E. Hartman, T. D. Green, J. B. Bateman, C. A. Senseney, and G. E. Hess, J. Appl. Phys. 24, 90 (1952)

21. K. L. Yudowitch, J. Appl. Phys. 20, 1232-1236 (1949)

22. J.W.M. DuMond, Phys. Rev. 72, 83-84 (1947)

23. W. J. West, Soc. Rheology, No. 25, Chicago, Illinois (October 1951)

24. C. H. Shaw, Report No. 8, Contract N6onr-22521, NR 017-606 (1951)

25. J. H. Munier, J. A. Bearden, and C. H. Shaw, Phys. Rev. 58, 537 (1940)

26. J.W.M. DuMond, Rev. Sci. Instr. 21, 188 (1950)

27. L. Shenfil, W. E. Danielson, and J.W.M. DuMond, Technical Report No. 15, ONR Contract N6onr-244, T.O. IV (NR 017-602) (1952)

28. L. Shenfil, W.E. Danielson, and J.W.M. DuMond, J. Appl. Phys. 23, 854 (1952)

29. Von R. Gwinner, Z. Physik 108, 523 (1938)

30. L. Y. Faust, Phys. Rev. 36, 161 (1930)

31. H. Hönl, Z. Physik 84, 1 (1933)

32. Larsson, Thesis, Upsala (1929)

33. E. C. Unnewehr, Phys. Rev. 22, 529 (1923)

34. A. H. Compton, Phys. Rev. 20, 84 (1922)

35. F. Holweck, Comptes Rendus 176, 570 (1923)

36. T. H. Laby, R. T. Bingham, and Shearer, Nature 122, 96 (1928)

37. H. E. Stauss, Phys. Rev. 31, 491 (1928)

38. H. W. Edwards, Phys. Rev. 32, 712 (1928)

39. T. H. Osgood, Rev. Mod. Phys. 1, 228 (1928)

40. N. Schön, Z. Physik 58, 3-4, 165 (1929)

41. H. E. Stauss, J. Opt. Soc. Am. 20, 616 (1930)

42. J. E. Henderson, Phys. Rev. 36, 785 (1930)

43. H. W. Edwards, Phys. Rev. 37, 339 (1931)

44. E. Derschem and M. Schein, Phys. Rev. 37, 1246 (1931)

45. J. L. Farrant, J. Appl. Phys. 21, 63 (1950)

46. C. B. O. Mohr, Proc. Roy. Soc. A133, 292 (1931)

47. T. H. Laby and R. T. Bingham, Proc. Roy. Soc. A133, 274 (1931)

48. J. M. Cork and J. A. Bearden, Phys. Rev. 39, 1 (1932)

49. J. M. Cork, Phys. Rev. 39, 193 (1932)

50. H. Hönl, Ann. Physik 18, 42, 625 (1933)

51. E. Dershem and M. Schein, Z. Physik 75, 5-6, 395 (1932)

52. P. Ewald and E. Schmid, Z. Krist. 94, 150 (1936)

53. W. Ehrenberg, Nature 160, 330 (1947)

54. W. Ehrenberg, J. Opt. Soc. Am. 39, 741, 746 (1949)

55. E. Prince, J. Appl. Phys. 21, 698 (1950)

56. A. H. Compton and S.K. Allison, X-Rays in Theory and Experiment (D. Van Nostrand Company, Inc., New York, 1934) p. 305

57. K. L. Yudowitch, J. Appl. Phys. 22, 214 (1951)

ACKNOWLEDGEMENT

Professor J. W. M. DuMond's love of scientific work and his keen interest in precise instrumentation have been a source of inspiration for which the writer will always be grateful. He would like to thank Professor DuMond for his invaluable assistance throughout this work. The writer would also like to thank Mr. Herbert Henrikson who made the mechanical lay-out for the total-reflection instrument, Mr. Raymond Burt who built this instrument, Mr. Theodore Garner, who assisted in the construction of the annular-slit instrument, and certainly his wife, Wilma, who has been a continual source of encouragement throughout this research.

This work was supported by the Office of Naval Research and the Atomic Energy Commission.